On modeling the Southern Ocean Phytoplankton Functional Types

Svetlana N. Losa[1,2], Stephanie Dutkiewicz[3], Martin Losch[1], Julia Oelker[4], Mariana A. Soppa[1], Scarlett Trimborn[1], Hongyan Xi[1], and Astrid Bracher[1,4]

[1]Alfred Wegener Institute Helmholtz Centre for Polar and Marine Research, Bremerhaven, Germany
[2]Shirshov Institute of Oceanology, Russian Academy of Sciences, Moscow, Russia
[3]Massachusetts Institute of Technology, Cambridge, Massachusetts, USA
[4]Institute of Environmental Physics (IUP), University of Bremen, Bremen, Germany

Correspondence: Svetlana Losa (Svetlana.Losa@awi.de)

Abstract. This study highlights recent advances and challenges of applying coupled physical-biogeochemical modeling for investigating the distribution of the key phytoplankton groups in the Southern Ocean, an area of strong interest for understanding biogeochemical cycling and ecosystem functioning under present climate change. Our simulations of the phenology of various Phytoplankton Functional Types (PFTs) are based on a version of the Darwin biogeochemical model coupled to the

5 Massachusetts Institute of Technology (MIT) general circulation model (Darwin-MITgcm). The ecological module version was adapted for the Southern Ocean by: 1) improving coccolithophores abundance relative to the original model by introducing a high affinity for nutrients and an ability to escape grazing control for coccolithophores; 2) including two different (small *vs.* large) size classes of diatoms; and 3) accounting for two distinct life stages for *Phaeocystis* (single cell *vs.* colonial). This new model configuration describes best the competition and co-occurrence of the PFTs in the Southern Ocean. It improves

10 significantly relative to an older version the agreement of the simulated abundance of the coccolithophores and diatoms with *in situ* scanning electron microscopy observations in the Subantarctic Zone as well as with *in situ* diatoms and haptophytes (including coccolithophores and *Phaeocystis*) chlorophyll a concentrations within the Patagonian Shelf and along the Western Antarctic Peninsula obtained by diagnostic pigment analysis. The modeled Southern Ocean PFT dominance also agrees well with satellite-based PFT information.

1 Introduction

15 The Southern Ocean is one of the most important regions in regulating climate via the sinking of CO_2 and, at the same time, is a region with the dynamics evidently altered by present climate change. The climatic changes in the Southern Ocean environmental conditions affect the spatial distribution of phytoplankton (Deppeler and Davidson, 2017). The phenology and dominance of different phytoplankton functional types (PFTs) sustaining the marine food web affect the diversity of higher

20 trophic levels. Playing distinct roles in biogeochemical cycling, PFTs also determine how and on which spatial and temporal scales the ocean mediates climate. The term "key Plankton Functional Types" was proposed for the ocean biogeochemical modelling community in the study by Le Quéré et al. (2005). The specific biogeochemical role of particular oceanic plankton (bacteria, phyto- and zoo-plankton) was one of the criteria chosen for distinguishing key plankton types among/across different

size (pico-, nano-, micro-), trophic and taxonomic groups. For instance, the importance of diatoms, the main phytoplankton
25 silicifiers, is related to the silica cycling and their high efficiency of carbon export through grazing, direct sinking of single
cells, and through mass sedimentation events (Le Quéré et al., 2005). The extent to which diatoms influence the ocean's
biological carbon pump depends on the silicification determined by size (from nano- to micro-) diversity within this functional
type (Tréguer et al., 2018). Coccolithophores, the main planktonic calcifiers, make a major contribution to the total content of
particulate inorganic carbon in the oceans (Milliman, 1993; Ackleson et al., 1988; Rost and Riebesell, 2004) through production
30 and release of calcium carbonate plates (coccoliths), and, therefore, also impact the alkalinity of the ocean. *Phaeocystis* as a
dimethyl sulfide producer alters the atmospheric sulfur cycle and similar to diatoms forms prominent blooms in the Southern
Ocean and supports export production. In the global ocean, the pico-phytoplankton group of N-fixers regenerates nutrients
and, therefore, influence the marine recycled production (Waterbury et al., 1986; Morán et al., 2004). The biogeochemical role
of pico-autotrophs including small eukaryotes and photosynthetic bacteria (*Prochlorococcus*, *Synechococcus*) is defined as a
35 substantial contributor to primary production in the oligotrophic regions and High Nutrients Low Chlorophyll areas.

The other two criteria considered by Le Quéré et al. (2005) for defining the key plankton functional types were directly
related to modeling requirements: 1) the biomass and distribution of the key planktonic type should be controlled by distinct
environmental conditions (hydrography, nutrients) and physiological parameters; 2) the dynamics of particular planktonic type
should impact distinctly the distribution of others (Le Quéré et al., 2005). For instance, while never known to be dominant in
40 the Southern Ocean, pico-phytoplankton occupying its particular ecological niche might alter the distribution extent of larger
phytoplankton groups. Thus, the term "functional" contains at least three aspects: 1) how the plankton type relates to the
biogeochemical processes; 2) how it adapts to the environmental conditions; and 3) how it alters biogeography of others. The
set of key Plankton Functional Types (PFTs) defined by Le Quéré et al. (2005) includes also heterotrophic bacteria, and three
groups of zooplankton. However, in the ocean color community that has been dealing with detecting photosynthetic plankton
45 – phytoplankton – the meaning of the abbreviation PFT has been transformed to Phytoplankton Functional Types.

The recognized need of understanding the variability and distribution of different PFTs has motivated some studies on
developing satellite based algorithms for PFTs retrievals (Sathyendranath, 2014; Mouw et al., 2017; Bracher et al., 2017) com-
plementary to the scarce number of available *in situ* observations (Peloquin et al., 2013; Buitenhuis et al., 2013b; Leblanc et al.,
2012; O'Brien et al., 2013; Vogt et al., 2012). In this respect, we have to emphasize that different satellite retrieval algorithms
50 as well as *in situ* measurements use various approaches not necessarily directly relating PFTs to its biogeochemical role or
functional type, but rather its morphological and/or optical features (Bracher et al., 2017). This fact provoked a discussion on
differences between differentiations among phytoplankton used in observations and assumed in biogeochemical models. In the
review by Bracher et al. (2017), the term "Phytoplankton Group" was introduced allowing to use, and emphasize, if required,
other classifications, for instance phytoplankton size class or taxonomic group. Hereafter, with the abbreviation PFT we refer
55 to Phytoplankton Functional Types and use the term "Phytoplankton Group" (PG) as a synonyme.

The studies by Le Quéré et al. (2005) and Follows et al. (2007) initiated efforts in numerical biogeochemical modeling
with key PFTs resolved explicitly given the thee aforementioned aspects of functionality. Some of the biogeochemical models
developed for the global ocean represent only two (diatoms and other nano-phytoplankton) or three (plus diazotroph/N-fixer)

PFTs (Hashioka et al., 2013; Vogt et al., 2013; Bopp et al., 2013; Hauck et al., 2013; Schourup-Kristensen et al., 2014;
60   Laufkötter et al., 2015) and only implicitly account for calcification (except for the study by Buitenhuis et al. 2013a where
coccolithophores were considered as a distinct phytoplankton group). The NASA ocean biogeochemical model (NOBM, Gregg
and Casey 2007; Gregg and Rousseaux 2016) includes four PFTs: diatoms, coccolithophores, cyanobacteria and chlorophytes.
The Darwin ecological model (Follows et al., 2007; Ward et al., 2012; Dutkiewicz et al., 2015) allows to represent more
than three (up to several thousands) phytoplankton groups (including the key types proposed by Le Quéré et al. 2005) in
65   accordance to their functional type, size class (Ward et al., 2012, 2017) and photophysiological/optical properties (Hickman
et al., 2010; Dutkiewicz et al., 2018). Since the Darwin model offers the highest potential to simulate globally relevant PFTs,
we use this model in our study to set up such a configuration that would allow best to describe the key Southern Ocean
phytoplankton groups but still keeping tractable computationally with only a handful of PFTs. The environmental conditions
related to phytoplankton growth are simulated by the Massachusetts Institute of Technology (MIT) ocean general circulation
70   model (MITgcm) coupled with a sea-ice model. We investigate: 1) whether this coupled sea-ice – ocean – biogeochemical
model is skillful enough to predict the distribution of diatoms, coccolithophores and *Phaeocystis* over the various dynamical
regions of the Southern Ocean; 2) the prerequisite for plausible simulations of their co-occurrence and temporal evolution;
and 3) how this model data on the Southern Ocean PFTs can complement available *in situ* and satellite observations with a
perspective to obtain long-term information. When determining the model requirements in diversity of assumed PFT traits we
75   hypothesise on biological factors explaining the observed Southern Ocean PFT biogeography.

The paper is organized as follows. Section 2 describes the numerical model set up, experimental design and observations (*in situ* and satellite retrievals) exploited for model evaluation, Section 3 presents the results and Section 4 the discussion. Section 5 concludes with summary and outlook.

2   Method

80   ### 2.1   Numerical Modeling

2.1.1   Biogeochemistry

The Darwin biogeochemical model represents ocean biogeochemical cycling of phosphorus (P), nitrogen (N), carbon (C), silicon (Si) and iron (Fe). Chlorophyll *"a"* (Chla) and carbon are decoupled given the Geider et al. (1998) photophysiological model. The version of the Darwin model used in our study simulates, among total 42 biogeochemical compartments describ-
85   ing these biogeochemical cycles, two types of zooplankton and six phytoplankton groups. These phytoplankton groups are
analogues of diatoms, nano-phytoplankton, prochlorophytes, other pico-phytoplankton (including pico-eukaryotes), nitrogen
fixing phytoplankton (including *Trichodesmium*) and coccolithophores. Starting from the setup of Dutkiewicz et al. (2015),
to adapt the Darwin model for realistic simulations of the Southern Ocean biogeochemistry and phytoplankton dynamics and
diversity, the following steps were performed:

90   Diatoms were represented by two distinct size classes (as two different model variables): small and "slightly silicified and fast growing" at lower latitudes (introduced instead of "other pico"); large and "strongly silicified slowly growing cells" at high latitudes (Queguiner, 2013);

Assumed coccolithophores physiology accounted for high affinity for nutrients (Paasche, 2001) and ability to escape grazing control (Huskin et al., 2000; Nejstgaard et al., 1997; Losa et al., 2006);

95   Other nano-phytoplanktonplankton (referred to as "other large" in the original Dutkiewicz et al. 2015) was presented by *Phaeocystis antarctica*. After performing several sensitivity experiments with different physiological traits assumed for the various phytoplankton types and allowing to simulate realistically co-occurrence of coccolithophores and *Phaeocystis*, two phases of the *Phaeocystis* life stages (colonies and solitary cells) were introduced following the parameterization used in Popova et al. (2007) and Kaufman et al. (2017).

100   Thus, the following six PFTs were considered, large and small diatoms, *Phaeocystis* and coccolithophores, *Proclorococcus*-like and N-fixers. In the current model configuration, instead of exploiting the radiative transfer model accounting explicitly for absorption and scattering of spectrally resolved light as in the version by Dutkiewicz et al. (2015), we used a simplified (because of computational limitations) parametrization of the light in terms of shortwave irradiance (I) penetrated over depth (z from vertical model grid level h_k to h_{k+1}):

$$I = \int_{h_k}^{h_{k+1}} I_k * e^{-(k_w + k_c Phy + k_{cdom} CDOM)z} dz, \tag{1}$$

where, k_w is the light attenuation coefficient due to water absorption (0.04 m^{-1}), k_c (m^2 mmol^{-1}) denotes attenuation due to phytoplankton (Phy, mmol m^{-3}), k_{CDOM} represents attenuation by the coloured dissolved organic matter (CDOM, mmol m^{-3}). k_{CDOM} is estimated as following:

$$k_{CDOM} = \int_{\lambda_{i=1}}^{\lambda_{i=K}} c_{cdom}(\lambda_0) * e^{-s_{cdom}(\lambda_i - \lambda_0)} d\lambda, \tag{2}$$

110   here, $c_{cdom}(\lambda_0)$ is the CDOM – specific absorption at reference waveband λ_0, s_{cdom} is the CDOM spectral slope (the values are taken from the study by Kitidis et al., 2006). As a result of integrating CDOM absorption over the spectral range from λ_1 = 400 nm to λ_K = 700 nm, k_{CDOM} is equal to 10 m^2 mmolP^{-1}.

Table 1 summarizes specific traits for the simulated PFTs, which is presented by the following physiological parameters: the maximum photosynthetic rate (P_{max}^C, day^{-1}); the photoinhibition parameter (β); the growth half-saturation constant (k_{sat},

115   mmol m^{-3}); the biomineralizing function ($mfunc$). These main differences between traits specified alter the growth (μ_j) of the particular phytoplankton (j = 1, 2,..., 6), grazing of phytoplankton by small or micro-zooplanktons (Gr_{jk}, k = 1, 2) given the palatability factor ($r_{j,k}$) and sinking (w_{sink}, $mday^{-1}$).

Growth is parameterized following Geider et al. (1998):

$$\mu_j = P_{mj}^C(1 - e^{-\frac{\alpha_j I \theta_j}{P_{mj}^C}}) \cdot f(\beta), \tag{3}$$

$$P_{mj}^C = P_{max_j}^C \gamma_T \gamma_\eta, \tag{4}$$

$$\alpha_j = \phi_{max_j} \overline{a_j^*}, \tag{5}$$

$$\gamma_\eta = min(\eta_{ji}), \eta_{ji} = f(k_{sat_i}) \tag{6}$$

here P_{mj}^C is the light saturated photosynthesis rate; γ_T and γ_η denote the functions of the growth rate on temperature and limiting nutrients (η_{ji}, $i = P, N, Si, Fe$), respectively; α_j is the initial slope of the photosynthesis *vs.* irradiance (P-I, Platt et al. 1980) curve, which is a product of the phytoplankton-specific light absorption (considered spectrally averaged, $\overline{a_j^*}$) and the maximum quantum yield of carbon fixation (ϕ_{max_j}); θ_j is the simulated chlorophyll to carbon ratio. The P_{mj}^C and k_{sat_i} parameters are specified with the use of empirical allometric relationships (Ward et al., 2012, 2017). Opposed to the study by Gregg and Casey (2007), Gregg and Rousseaux (2016), the γ_T function was considered the same for diatom, coccolithophores, *Phaeocystis* and prokaryotes.

Grazing is formulated as a Holling II function:

$$Gr_{jk} = g_{max_{jk}} \gamma_T \frac{r_{jk} Phy_j}{G_k} \frac{G_k^2}{G_k^2 + \kappa_{sat_k}^2}, \tag{7}$$

$$G_k = \sum_j r_{jk} Phy_j, \tag{8}$$

where $g_{max_{jk}}$ is the zooplankton maximum grazing rate on phytoplankton, and κ_{sat_k} is the half-saturation constant for grazing. *Sinking* is expressed given the phytoplankton-specific sinking rate w_{sink_j} as

$$Phy_{sink} = \frac{\partial w_{sink_j} Phy_j}{\partial z}. \tag{9}$$

The described biogeochemical model configurations given the parameters in Table 1 was exploited for a reference experiment (REF). In an additional experiment (PHAEO), two *Phaeocystis* life stages were considered as a function of iron availability (Bender et al. 2018): if the iron concentration is less than the iron half saturation constant (k_{satFe}), *Phaeocystis* is assumed to be present as solitary cells with the mortality rate and grazing pressure being higher by 1.3 and 1.25, respectively, than those cells in a colonial form. Following Popova et al. (2007), we considered *Phaeocystis* sinking rate (w_{sink}) dependent of available nutrients, but in our case it was limited to iron concentration as following

$$w_{sink}(Phaeo) = w_{sink}(1 - Fe/(Fe + k_{satFe})), \tag{10}$$

$$k_{satFe}(Phaeo_{cell}) = k_{satFe}(Phaeo) * 0.8. \tag{11}$$

Note, that in the model *Phaeocystis* is still the same variable/array, but the assumed morphology and, therefor, physiology different for the different life stages of *Phaeocystis*.

5

2.1.2 Physics

The biogeochemical model was coupled to the MITgcm circulation model (MITgcm Group, 2012) in a configuration based on a cubed-sphere grid (Menemenlis et al., 2008) with mean horizontal spacing of 18 km and 50 vertical levels with the resolution ranging from 10 m near the surface to 450 m in the deep ocean (as in Taylor et al. 2013). The model was forced by 3-hourly

150 atmospheric conditions from the Japanese 55-year reanalysis (JRA55, Kobayashi et al. 2015) over the time of 1999 – 2012 following a spin up period 1992 – 1998. Our configuration of the MITgcm was similar to the configuration used by Taylor et al. (2013) to examine the mechanisms behind the phytoplankton bloom in the Antarctic seasonal ice zone.

The available light and light penetration depend on present ice conditions:

$$Q_{sw,net} = Q_{sw,water} * (1-c) + Q_{sw,ice} * c, \tag{12}$$

155 $$Q_{sw,ice} = 0.3 * Q_{sw} * (1-\alpha_{ice}) e^{-1.5 h_{ice}}, \tag{13}$$

where c is the fractional ice cover, h_{ice} is the ice thickness, α_{ice} is the sea ice albedo. Q_{sw} denotes the incoming shortwave radiation, $Q_{sw,net}$ is the net downward shortwave heat flux as a result of water and ice fractions ($Q_{sw,water}$ and $Q_{sw,ice}$, respectively). However, the light does not penetrate if the ice is covered by snow.

2.1.3 Biogeochemical tracers initialisation

160 To initialise (in 1992) the biogeochemical model variables evolved in cycling N, C, Fe, Si (including inorganic and organic particular and dissolved pools) and Chla, we used the results of the study by Taylor et al. (2013), since these variables are presented in both models, Darwin and the Regulated Ecosystem Model (REcoM, Schartau et al. 2007) used in Taylor et al. (2013). The model variables describing the phosphorus cycle were initialised given N-based variables and the Redfield N:P ratio. The REcoM-based phytoplankton and zooplankton biomasses from Taylor et al. (2013) were distributed equally between

165 six and two Darwin PFTs and zooplankton groups, respectively.

2.2 Evaluation with observational data

2.2.1 *In situ* observations

As independent information on phytoplankton distribution, we used Chla of diatoms, haptophytes and prokaryotes from a global data set available at https://doi.pangaea.de/10.1594/PANGAEA.875879 (Soppa et al., 2017). The data was derived from

170 *in situ* high precision liquid chromatography (HPLC) pigment measurements using the Diagnostic Pigment Analysis (DPA) following Vidussi et al. (2001) and Uitz et al. (2006) and modified as in Hirata et al. (2011) and Brewin et al. (2015) and adapted to a much larger data set. For more details, we refer the reader to the study by Losa et al. (2017, Supplementary Material, Section 1). Table 2 contains the information about evaluated phytoplankton groups as classified in the model and observations. It is worth mentioning that the DPA allows also to retrieve other phytoplankton groups – like dinoflagellates,

175 cryptophytes and green algae – however, they were not included into the referred data set and not considered in our study.

Figure 1 shows the locations of the available *in situ* data in the Southern Ocean. To support discussions on the biogeography of the observed and simulated PFTs, this figure also depicts several biogeochemical provinces (Longhurst, 1998) distributed over the Southern Ocean: Austral Polar Province (APLR), Antarctic Province (ANTA), Subantarctic Water Ring Province (SANT), South Subtropical Convergence Province (SSTC), Humbold Current Coastal Province (CHIL), Southwest Atlantic

180 Shelves Province (FKLD), Eastern Africa Coastal Province (EAFR), Australia-Indonesia Coastal Province (AUSW), East Australian Coastal Province (AUSE). The system of the Southern Ocean fronts (Orsi et al., 1995) – the Sub-Antarctic Front (SAF), the Polar Front (PF), the Southern Antarctic Circumpolar Current Front (SACCF) and the Southern Boundary of ACC (SBDY) - is also shown. Simulated PFTs were additionally compared to measurements reported by Smith et al. (2017) which were obtained by scanning electron microscopy.

185 **2.2.2 Remote sensing**

Model results were evaluated based on phytoplankton dominating groups from the climatological monthly mean satellite derived product PHYSAT. This product based on the multispectral Sea-Viewing Wide Field-of-View Sensor (SeaWiFS) information was developed by Alvain et al. (2008) and available on http://log.cnrs.fr/Physat-2?lang=fr. We also used the Chla retrieved for three PFTs with differential optical absorption spectroscopy (PhytoDOAS, Bracher et al. 2009; Sadeghi et al.

190 2012) given hyperspectral information from the Scanning Imaging Absorption Spectrometer for Atmospheric Chartography (SCIAMACHY, Bracher et al. 2017; https://doi.org/10.1594/PANGAEA.870486) and the SynSenPFT Chla data product (Losa et al. 2017, https://doi.org/10.1594/PANGAEA.875873). The SynSenPFT product is a combination of PhytoDOAS Chla for diatoms and coccolithophores and OC-PFT Chla for diatoms and haptophytes derived with an abundance-based approach (Hirata et al. 2011, further refined in Soppa et al. 2014) applied to multi-spectral satellite based total Chla from the Ocean

195 Colour Climate Change Initiative (OC-CCI version 2, https://rsg.pml.ac.uk/thredds/catalog-cci.html, OC-CCI 2015). While PhytoDOAS product from the SCIAMACHY sensor are only available at 0.5° horizontal resolution as monthly mean Chla, the SynSenPFT allows by the combination of PhytoDOAS with OC-PFT multispectral data at a daily 4 km resolution. Respectively, PhytoDOAS and PHYSAT satellite products were derived based on phytoplankton absorption properties captured by the satellite sensors and distinguished by the retrieval algorithms either as a particular PFT optical imprint ("finger print") in

200 case of available hyperspectral information (in PhytoDOAS) or as anomalies in a multispectral signal (in PHYSAT). Thus, the PhytoDOAS allows to retrieve quantitatively major PFTs (coccolithophores, diatoms, cyanobacteria), while PHYSAT provides information about the dominant phytoplankton among five PGs: prokaryotes (presented by *Prochloroccocus* and *Synechococcus*-like SCL), diatoms, haptophytes in general and *Phaeocystis* in particular.

3   Results and Discussions

205   3.1   Improved diatom phenology: diversity within diatoms

Figure 2 shows PFT dominance retrieved by PHYSAT and simulated by Darwin-MITgcm Dutkiewicz et al. (2015) version for July and January. It is seen that, in comparison with PHYSAT, modeled diatoms were misrepresented in the Southern Ocean during austral summer. In July simulated diatoms were dominant in the Atlantic section of subantarctic zone, opposed to observed dominance of haptophytes. This disagreement between simulations and satellite observations indicates model deficien-
210   cies in representing PFT phenology and distribution. Generally, the model overestimated the dominance of small non-silicified phytoplankton. A series of Darwin-MITgcm experiments, with different model configurations with respect to assumed PFTs and their traits described by various physiological parameters, have been conducted for the global ocean and evaluated for the Southern Ocean over the period of 1999 – 2012. The detailed protocol of the experiments can be found in the Supplementary Material (Section S1). The best simulations, in terms of agreement with observed phytoplankton composition (Trimborn et al.,
215   2015) and dominance (PHYSAT, Alvain et al. 2008) and diatom phenology (Soppa et al., 2016b), were performed with prescribing two size classes of diatoms (large and small, Queguiner 2013; Tréguer et al. 2018) given the parameters in Table 1 but initially without considering *Phaeocystis* in two distinct phases. Figure 2 illustrates the model phytoplankton dominance obtained for July 2003 and January 2004 for this reference (REF) experiment. One can notice a significant improvement in the model PFT dominance agreement with the PHYSAT product as compared to those previously reported (Dutkiewicz et al.,
220   2015). These results suggest that the too early (relative to observations) appearance of diatom blooms in the Southern Ocean simulated by most (global ocean) biogeochemical models (Vogt et al. 2013; as well in the Darwin model set up published in the study by Dutkiewicz et al. 2015) could be explained by lack of inclusion of the size diversity in diatoms (Tréguer et al., 2018).

3.2   Co-occurrence of coccolithophores and diatoms

225   This augmentation of the biogeochemical module by two size classes of diatoms appeared to be a prerequisite for the realistic simulation of the abundance of diatoms and coccolithophores in the Subantarctic Zone. Figure 3 shows the Southern Ocean spatial distribution of Chla for small and large diatoms, coccolithophores and "other large" (*Phaeocystis*-like) phytoplankton in January 2004, which is in agreement with the observations by Signorini et al. (2006), Balch et al. (2016) and Smith et al. (2017). The figure illustrates the co-occurrence of model simulated diatoms and coccolithophores as observed north of the
230   Subantarcic Front (Smith et al., 2017). The results are supported by the PhytoDOAS PFT retrievals from SCIAMACHY hyperspectral information (Bracher et al. 2017, https://doi.org/10.1594/PANGAEA.870486) and SynSenPFT product (Losa et al. 2017, https://doi.org/10.1594/PANGAEA.875873), as presented for the related time frame and region in Losa et al. (2018, https://oceanopticsconference.org/extended/Losa_Svetlana.pdf). However, it is worth emphasizing that model representation of co-existence/competition within the haptophytes group (coccolithophores vs. *Phaeocystis*) still remained a challenge: small
235   changes in the Darwin model physiological parameters led to loss of either *Phaeocystis* or coccolithophores. For instance, in experiment REF to the end of the considered period of time, coccolithophores did not survive.

3.3 Differentiation among haptophytes: coccolithophores *vs. Phaeocystis*

To cope with the aforementioned "chaoticity" (Popova et al., 1997) of the system leading to two different states either with coccolithophores or with *Phaeocystis ant.* existent, in experiment PHAEO we introduced additional differences in the traits of

240 these two PFTs. In particular, we considered two distinct life stages of *Phaeocystis ant.* (colonies and solitary cells) in which its morphological features and physiology depend on iron availability (Bender et al., 2018)). To illustrate the simulated Southern Ocean phytoplankton compositions, we calculated zonally averaged ratios of individual PFT biomass to summed biomass over all simulated PFTs for the following four sectors of the Southern Ocean: the Atlantic Ocean sector (AOS, $60^oW - 18^oE$), the Indian Ocean sector (IOS, $18^oE - 120^oE$), Australian sector (AST, $120^oE - 180^oE$) and the Pacific Ocean sector (POS, 180^oE

245 $- 60^oW$). Figure 4 presents these meridional distributions of the different PFTs in February 2008 for experiments with and without considering *Phaeocystis* in two different life stages (we refer to these experiments as PHAEO and REF, respectively). One can see that in experiment REF, "other large" (including *Phaeocystis*) outcompetes coccolithophores leading to too low concentrations of coccolithophores south of the Polar Front, while small diatoms exist there in both experiments (however, in different percentages). Experiment PHAEO reveals more plausible meridional distributions of the phytoplankton composition

250 with respect to the coccolithophores fractions gradually increasing in the direction to the north of the Subantarctic Front, where it reaches ~30% of the total biomass. This result agrees with the estimates of Smith et al. (2017) obtained for January – February – March. Seasonal variations of the PHAEO phytoplankton compositions are shown in the Supplementary Material (Section S4, Figure S8). As seen in this figure, the fraction of coccolithophores is higher in austral winter.

Differences in the biomass distribution between coccolithophores, *Phaeocystis* and diatoms influence zooplankton abun-

255 dances as prescribed by the model assumptions and parameterisations (Figure 4, blue curve). In this respect, we have to emphasize that the realistic coccolithophores distribution was obtained as a result of reduced grazing pressure on this PFT among other circumstances. This contradicts the study by Nissen et al. (2018), who reported on an increased grazing of coccolithophores as a factor controlling the coccolithophores phenology in the Southern Ocean. However, our results are supported by studies by Nejstgaard et al. (1997), Huskin et al. (2000) and Losa et al. (2006). In the study by Losa et al. (2006) on optimised

260 biogeochemical parameters the authors showed that the coccolithophores bloom was associated with low grazing pressure. Based on their laboratory experiments, Nejstgaard et al. (1997) and Huskin et al. (2000) concluded that coccolithophores (due to its "stony" structure) do not influence the microzooplankton growth. High affinity of coccolithophores for nutrients (for phosphate and iron to a larger extent than for nitrogen, Paasche 2001) makes them strongly competitive in environmental conditions with declining nutrient concentrations (Paasche, 2001; Iglesias-Rodríguez et al., 2002), for instance under strong ocean

265 stratifications or nutrient consumption by other PFTs (see Figure 5).

Figure 5 depicts the Chla spatial distribution for diatoms, *Phaeocystis* and coccolithophores for January and March 2004. This figure clearly shows the co-occurrence of diatoms and coccolithophores in the Subantarctic Zone north of the Subantarctic Front, as well as co-existence of simulated diatoms and *Phaeocystis* south of the Polar Front. Figure 5 also presents the spatial distribution of silicon, dissolved iron and phosphate in March 2004 (agreed well with the World Ocean Atlas, Garcia et al.

270 2014). The regions with high iron concentrations (in the Ross Sea, along the Western Antarctic Peninsula, around the Falkland,

South Georgia and South Sandwich, Crozet and Kerquen Islands) indicates the area of *Phaeocystis ant.* potential existence in colony form. Thus Figure 5 shows that the simulated abundance of coccolithophores north of the Subtropical Front (STF) – where phosphate occurs in very low concentrations – is explained by the introduced high affinity of this PFT to phosphate (small half-saturation rate in γ_η function) allowing coccolithophores to grow in nutrient depleting conditions. However, in the region

275 between the Subtropical and Subantarctic Fronts the occurrence of coccolithophores is more evidently linked to low grazing pressure on this PFT, due to its much lower palatibility for zooplankton in comparison with small diatoms or *Phaeocystis* presented by single solitary cells. As reported by Smith et al. (2017), the simulated coccocolithophores is distributed over the silica-depleted area. However, in the model world this PFT is not directly constrained by this nutrient, opposed to diatoms.

Figure 6 illustrates the implication of the differences in the distribution among the haptophytes on the carbon cycling as

280 carbon distributed into different inorganic and organic, particulate and, consequently, dissolved pools. Shown are the particulate inorganic carbon (PIC) and particulate organic matter (POC) for the experiments REF and PHAEO in March 2004. As seen, opposed to REF in the experiment PHAEO we obtained higher concentration of POC south of the Southern Antarctic Circumpolar Current Front but less POC and higher PIC concentrations north of the Subantarctic Front, which is in agreement with (Balch et al., 2005, 2016).

285 **3.4 Experiment PHAEO: General evaluation**

3.4.1 PHAEO dominance against PHYSAT and SynSenPFT

Similar to Figure 2, Figure 7 depicts model phytoplankton dominance obtained for June - August 2003, December 2003 and January – February 2004 but for the experiment PHAEO. As for the experiment REF, PFT dominance agrees with PHYSAT data product better than the model results of Dutkiewicz et al. (2015). However, the results differ from the REF dominance: In

290 July and January, the extent of diatom dominance around the Antarctic is wider, further to the north and around the Kerguelen Islands; less extension of the diatom dominance in the Atlantic Section north of SAF, showing even larger agreement to PHYSAT.

Figure 8 presents the spatial distribution monthly means of simulated surface Chla for coccolithophores and diatoms over the region from 30°S to 70°S and from 70°W to 120°E as shown in the study by Smith et al. (2017). These model results

295 are compared with Chla obtained for the same domain and time period with SynSenPFT algorithm (Losa et al., 2017). The simulated coccolithophores distribution reveals a smaller "belt" in comparison with SynSenPFT with well-agreeing northern boundaries, but not extending further south of the Polar Front. For diatoms, modeled Chla exceeds SynSenPFT estimates south of the Antarctic Circumpolar Current front. In this respect, it is worth emphasizing that SynSenPFT product at the latitudes higher than 60°S is mostly influenced by OC-PFT estimates because of much less available SCIAMACHY information. (see

300 Supplementary Material, Section S2). OC-PFT retrievals (Losa et al., 2017) contain information generally on haptophytes (not specifically on coccolithophores). Moreover, PhytoDOAS coccolithophores retrievals are based on coccolithophores specific absorption spectrum that is, indeed, very similar to the specific absorption spectrum of *Phaeocystis*. As seen from Figures 5 and 4 model simulations support the evidence of *Phaeocystis* dominance among haptophytes at these latitudes. SynSenPFT

diatom Chla is known to be underestimated for the Antarctic Province (see SynSenPFT PVR 2016, Soppa et al. 2016a).

305 However, diatom Chla estimates obtained with PhytoDOAS are higher (see Supplementary Material, Section S2) despite the low coverage of the product.

3.4.2 PHAEO against *in situ* observations

For a more precise comparison of the PHAEO model simulations with *in situ* information, Figures 9 – 10 and 11 show spatial distributions of model surface Chla for diatoms, haptophytes (including coccolithophores and *Phaeocystis*) and pico-

310 phytoplankton (cyanobacteria or prokaryotes) as (several selected) model snapshots with *in situ* observations available within a time window ± 1 week. The *in situ* Chla is depicted also at the same figure panels as coloured circles. A complete series of model snapshots depicting the spatial distribution of Chla for diatoms (large + small), haptophytes and prokaryotes against *in situ* observations (if available) has been collected over the time period from August 2000 to April 2012 and compiled as three video files (registered via AV-Portal of the German National Library of Science and Technology (TIB, see Video

315 supplement). These movies also nicely illustrate the PFT phenology. In Figure 9 and 10, the *in situ* observations (indicated by circles) match well the representing model Chla of diatoms and haptophytes in the area close to the Antarctic Peninsula and in the Southwest Atlantic Shelves biogeochemical province (FKLD, Longhurst, 1998), which illustrates a good agreement between the model and observations. In the Ross Sea, however, the model performance is less accurate for both diatoms and haptophytes (Figure 10, first panel, see also Vogt et al. 2012). In general, for the entire Southern Ocean the mean absolute

320 deviation of model Chla from observations (mean absolute error, MAE) is 0.74 mg m^{-3} and 0.22 mg m^{-3} for diatoms and haptophytes, respectively. The statistical estimates were obtained based on the model and observation match-ups within ± 1 week. Moreover, the model does not explicitly represent sea-ice algae and, therefore, might work less well in the region around the sea-ice.

As additional information on the agreement between model and observations, in the Supplementary Material Figures S9 and

325 S10 present frequency distributions of diatoms and haptophytes Chla for the simulations and measurements and the frequency distribution of the model and data differences. The latter shows that statistical criteria, such as mean absolute error (MAE) and root mean squared error (RMSE) give statistical meaningful metrics with respect to "model minus *in situ* Chla data" and the evaluation does not necessarily require a logarithmic transformation, as it is often done in ocean colour product validation (Brewin et al., 2010; Losa et al., 2017).

330 Tables 3 and 4 present the statistics of the model to *in situ* data comparison for diatoms and haptophytes Chla at several Longhurst's biogeochemical provinces (Longhurst 1998, see Figure 1). The worst statistics were obtained for diatoms in the Atlantic Sector of the ANTA province, where the simulated diatom Chla is systematically overestimated by ~0.5 mg m^{-3}. With respect to the agreement between model and observed *in situ* Chla for pico-phytoplankton depicted in Figures 11 and Figure S11 (in Supplementary Material) one can conclude that their frequency distributions differ, and the frequency distribution of the

335 differences confirms that MAE and RMSE given absolute (Table 5) or logarithmically transformed values can hardly provide satisfactory estimates. Nevertheless, it is worth emphasizing that the largest differences between model and observed *in situ* pico-phytoplankton are located along the Antarctic Peninsula. In this respect, we have to point out that all the statistics are

11

presented for a qualitative assessment of the model rather than for a quantitative estimates of model uncertainties, since the representation error (Janjić et al., 2018) related to the differences in spatial and temporal scales considered and sampled by the
340   model *vs.* observations as well as to the mismatch in grouping phytoplankton (Bracher et al., 2017) are still quite large.

4   Concluding remarks and outlook

Leveraging satellite estimates and *in situ* observations allowed us to define the trait requirements for capturing phytoplankton biogeography in the Southern Ocean. We set up a model for simulating the distribution of key Southern Ocean PFTs: diatoms, coccolithophores and *Phaeocystis*. The observed co-occurrence of two different phytoplankton groups, coccolithophores and
345   diatoms, in the Subantarctic Zone (Queguiner, 2013; Smith et al., 2017) was clearly simulated by the Darwin-MITgcm model adjusted for the Southern Ocean and in a reasonable agreement with PHYSAT, PhytoDOAS and SynSenPFT satellite products.

The Southern Ocean adjustment of the Darwin-MITgcm required introducing two size classes of diatoms (small *vs.* large) and improved coccolithophores physiology (which indeed might support a biochemical/physiological hypothesis on the coccolithophores distribution in the Southern Ocean). The simulated biogeography of coccolithophores was not controlled by
350   temperature itself, which was also found in the study by Smith et al. (2017). Neither it was directly explained by silica depleting, but phosphate as well as by low palatability of this PFT for grazers. The simulation of co-occurrence of coccolithophores and *Phaeocystis* required additional model developments. Thus, as a first trial, the Darwin model was augmented to account for changes in assumed life stage of *Phaeocystis ant.* (Popova et al., 2007; Kaufman et al., 2017) subject to iron availability (Bender et al., 2018). This parameterization of morphological shifts did indeed allow for co-existence of the two types
355   of haptophytes. However, there is still room for improvement. For instance, for specifying more precisely the differences in photophysiology and related optical imprints (Moisan and Mitchell, 2018) for *Phaeocystis* in cells and colonies phases. Below we highlight several crucial points that have to be considered in future and, if addressed, could potentially guide further model developments and lead to improved PFTs distribution simulations:

Phytoplankton growth: equation (6) *(ϕ_{max}).* The differences in the phytoplankton growth are presented mostly by the
360   variety of the assumed maximum photosynthesis rate ($P^C_{max_j}$) and chlorophyll to carbon ratio θ_j, resulting in slower growth of coccolithophores than for diatoms and *Phaeocystis*, which determines the simulated PFT phenology and competition. The initial slope of the P-I curve (α), opposed to the study by Hickman et al. (2010) and Dutkiewicz et al. (2015), was considered identical for all PFTs. The use of PFT specific absorption spectra (Eq. (6)) when setting up the PFT traits allows the initial slope of the P-I curve (α) being distinct for particular phytoplankton. However,
365   realistic representation of the α parameter would also require some differences in the maximum quantum yield of carbon fixation (ϕ_{max}) specification (Hiscock et al., 2008). This would further improve the model performance (for instance, *Phaeocystis ant.* dominance in the Ross Sea) and would probably bring the assumed $P^C_{max_j}$ values (which are currently, to some extent, overestimated) closer to measurements (*Tables S5, S6 Supplementary Material, Section S4*). However, the ϕ_{max} is measured given α and phytolankton specific absorption. That means that in the model world we have to
370   differentiate between the α parameter for distinct PFTs.

Prokaryotes: Even though the *Prochlorophytes*-analogue is not present/dominant in the Southern Ocean, accounting for this pico-phytoplankton is a prerequisite for the simulation of the northern edge of coccolithophores distribution south of the STF (in the SSTC bgc province). In this respect the assumption on photoinhibition for this PFT as well as for other PFTs might need a careful revision.

375 *Remineralisation and other parameterised processes:* The simulated distribution, competition and co-occurrence of the key Southern Ocean PFTs are generally discussed in terms of differentiating the PFT traits via the specification of phytoplankton growth (with different light acclimation strategies and affinities to nutrients) and palatibilities for zooplankton grazing. However, there are other processes altering the model PFT dynamics. For instance (a model based evidence, not shown), augmenting the model by CDOM affects the remineralisation processes affecting the nutrients distribution and

380 therefore the spatial and temporal distribution of PFTs competing for the available resources. One should also think of better representation of algae/sea-ice interaction.

Present-day satellite retrieval algorithms allow to detect biomass (and dominance) of some PFTs including haptophytes in general (OC-PFT, Hirata et al. 2011), coccolithophores in particular (PhytoDOAS, Sadeghi et al. 2012), diatoms and cyanobacteria/prokaryotes (OC-PFT; PhytoDOAS, Bracher et al. 2009). Several efforts have been made in deriving more specifically

385 green algae and dinoflagellates (see Xi et al. 2018; Hirata et al. 2011; Shang et al. 2014). Even though there is still the mismatch between the phytoplankton grouping used in numerical models, satellite algorithms and *in situ* observations, the information from these different sources becomes closer and, indeed, can be considered complementary.

However, when combining or comparing models and observational information, we have to keep in mind representation errors and limitations of approaches used for deriving PFT information from *in situ* and satellite observations. Generally,

390 a temporal and spatial scale mismatch exists between *in situ* or satellite observations and model output depending on the model discretization. *In situ* measurements in the Southern Ocean are sparse in space and time and only provide a fraction of the information obtained by the model. Satellite observations cover larger areas frequently but only cloud-free scenes which leads to a temporal bias in the often cloud-covered Southern Ocean. In addition, they are limited to only observe the first optical depth, which often limits the detection of the chlorophyll maximum. The development of algorithms for deriving

395 PFT information requires a large *in situ* dataset with homogeneous temporal and spatial distribution. Nevertheless, scientific cruises in the Southern Ocean are often carried out close to the continents/ice shelf or in regions with high phytoplankton concentration (Figure 1). The diagnostic pigment analysis used to estimate PFTs from HPLC pigments assumes that different PFTs have different marker pigments, but it is known that they can also have pigments in common (Hirata et al. 2011). This ambiguity leads to uncertainties in the *in situ* database which is, on the one hand, needed as fundamental input for the

400 algorithms of PFT retrievals and, on the other hand, used for direct comparison with model output here. Concerning spectral based methods applied to either *in situ* or satellite data, it is difficult to distinguish the specific absorption spectra of PFTs (e.g., coccolithophores and *Phaeocystis*). These and more limitations are well discussed by Sathyendranath (2014) and Bracher et al. (2017).

The evidence that biogeochemical modelling can capture phytoplankton specific traits in the way that it considers differ-
405   ent aspects of differentiation among phytoplankton groups – biogeochemical role; allometric, photophysiological and optical
parameters; accounting for carbon and Chla decoupling – makes the coupled ocean/biogeochemical models a very valuable
and skilful instrument that combines the knowledge from *in situ* measurements and remote sensing by exploiting various
PFT retrievals principles used (separately) in these observations and relates it to the environmental conditions. Further exten-
sion/progress could be expected given the radiative transfer model coupled to the biogeochemical model Gregg and Rousseaux
410   (2016) and Dutkiewicz et al. (2018) allowing to simulate spectrally resolved water leaving radiance and therefore providing
perspectives to assimilate explicitly multi- and hyper-spectral satellite information and correct if necessary the simulated PFTs
as the main water optical constituents.

5   Supplementary Material

The supplementary material contains a protocol of prior Darwin sensitivity experiments with differently prescribed phyto-
415   plankton traits (Section S1); PhytoDOAS diatoms Chla over the Great Calcite Belt (Section S2); seasonal variation of the
meridional distribution of zonally averaged phytoplankton composition for four sections of the Southern Ocean (Section S3);
in situ and laboratory measurement information on the photophysiological parameters of diatoms and *Phaeocystis* (Section S4);
and additional information on model evaluation against *in situ* (Section 5). Additionally there are three video files registered
via AV-Portal of the German National Library of Science and Technology (TIB), Hannover (doi to be provided).

420   *Code and data availability.* The model data were generated with the MIT Darwin Project Biogeochemical, Ecosystem, and OpticalModel.
The code is part of the MITgcm, which is available fromhttp://mitgcm.org. The specific version of the code used in this study, as well as initial
fields can be provided opon request from the corresponding author (svetlana.losa@awi.de). Information about observational data availability
is provided in the text (via specified URL).

Video supplement. The following three video files are available via AV Portal of German National Library of Science and Technology
425   (TIB, Hannover): Simulated distribution of diatom chlorophyll concentration in the Southern Ocean, https://doi.org/10.5446/42871; Simu-
lated distribution of haptophytes chlorophyll concentration in the Southern Ocean, https://doi.org/10.5446/42873; Simulated distribution of
prokaryotes chlorophyll concentration in the Southern Ocean, https://doi.org/10.5446/42872.

Competing interests. The authors declare that they have no conflict of interest.

Author contributions. AB: funding and PhySyn project lead; SL: conception and design of the experiments, compilation of the first draft

430 of the manuscript and updates according critical revisions by all the co-authors; SD, ML, SL: model development and set up; SD, ST and SL: PFT traits; MS, HX: *in situ* PFT Chla data processing and interpretation; AB and JO: satellite retrievals; all co-authors: substantial participation in analysis and discussion of the results and their implications.

Biogeosciences
Discussions

References

Ackleson, S., Balch, W., and Holligan, P.: White waters of the Gulf of Maine, Oceanography, 1, 18–22, 1988.

445   Alvain, S., Moulin, C., Dandonneau, Y., and Loisel, H.: Seasonal distribution and succession of dominant phytoplankton groups in the global
         ocean: A satellite view, Global Biogeochemical Cycles, 22, https://doi.org/10.1029/2007GB003154, 2008.

Balch, W. M., Gordon, H. R., Bowler, B. C., Drapeau, D. T., and Booth, E. S.: Calcium carbonate measurements in the sur-
         face global ocean based on Moderate-Resolution Imaging Spectroradiometer data, Journal of Geophysical Research: Oceans, 110,
         https://doi.org/10.1029/2004JC002560, 2005.

450   Balch, W. M., Bates, N. R., Lam, P. J., Twining, B. S., Rosengard, S. Z., Bowler, B. C., Drapeau, D. T., Garley, R., Lubelczyk, L. C., Mitchell,
         C., and Rauschenberg, S.: Factors regulating the Great Calcite Belt in the Southern Ocean and its biogeochemical significance, Global
         Biogeochemical Cycles, 30, 1124–1144, https://doi.org/10.1002/2016GB005414, 2016.

Bender, S. J., Moran, D. M., McIlvin, M. R., Zheng, H., McCrow, J. P., Badger, J., DiTullio, G. R., Allen, A. E., and Saito, M. A.:
         Colony formation in *Phaeocystis antarctica*: connecting molecular mechanisms with iron biogeochemistry, Biogeosciences, 15, 4923–
455   4942, https://doi.org/10.5194/bg-15-4923-2018, 2018.

Bopp, L., Resplandy, L., Orr, J. C., Doney, S. C., Dunne, J. P., Gehlen, M., Halloran, P., Heinze, C., Ilyina, T., Séférian, R., Tjiputra, J., and
         Vichi, M.: Multiple stressors of ocean ecosystems in the 21st century: projections with CMIP5 models, Biogeosciences, 10, 6225–6245,
         https://doi.org/10.5194/bg-10-6225-2013, 2013.

Bracher, A., Vountas, M., Dinter, T., Burrows, J. P., Röttgers, R., and Peeken, I.: Quantitative observation of cyanobacteria and diatoms from
460   space using PhytoDOAS on SCIAMACHY data, Biogeosciences, 6, 751–764, https://doi.org/10.5194/bg-6-751-2009, 2009.

Bracher, A., Bouman, H. A., Brewin, R. J. W., Bricaud, A., Brotas, V., Ciotti, A. M., Clementson, L., Devred, E., Di Cicco, A., Dutkiewicz,
         S., Hardman-Mountford, N. J., Hickman, A. E., Hieronymi, M., Hirata, T., Losa, S. N., Mouw, C. B., Organelli, E., Raitsos, D. E., Uitz,
         J., Vogt, M., and Wolanin, A.: Obtaining Phytoplankton Diversity from Ocean Color: A Scientific Roadmap for Future Development,
         Frontiers in Marine Science, 4, 55, https://doi.org/10.3389/fmars.2017.00055, 2017.

465   Bracher, A., Dinter, T., Wolanin, A., Rozanov, V. V., Losa, S., and Soppa, M. A.: Global monthly mean chlorophyll a surface concentrations
         from August 2002 to April 2012 for diatoms, coccolithophores and cyanobacteria from PhytoDOAS algorithm version 3.3 applied to
         SCIAMACHY data, link to NetCDF files in ZIP archive, https://doi.org/10.1594/PANGAEA.870486, https://doi.org/10.1594/PANGAEA.
         870486, in supplement to: Losa, Svetlana; Soppa, Mariana A; Dinter, Tilman; Wolanin, Aleksandra; Brewin, Robert J W; Bricaud, Annick;
         Oelker, Julia; Peeken, Ilka; Gentili, Bernard; Rozanov, Vladimir V; Bracher, Astrid (2017): Synergistic Exploitation of Hyper- and Multi-
470   Spectral Precursor Sentinel Measurements to Determine Phytoplankton Functional Types (SynSenPFT). Frontiers in Marine Science,
         4(203), 22 pp, https://doi.org/10.3389/fmars.2017.00203, 2017.

Brewin, R. J., Sathyendranath, S., Hirata, T., Lavender, S. J., Barciela, R. M., and Hardman-Mountford, N. J.: A three-component model of
         phytoplankton size class for the Atlantic Ocean, Ecological Modelling, 221, 1472–1483, https://doi.org/10.1016/j.ecolmodel.2010.02.014,
         2010.

475   Brewin, R. J., Sathyendranath, S., Jackson, T., Barlow, R., Brotas, V., Airs, R., and Lamont, T.: Influence of light in the mixed-
         layer on the parameters of a three-component model of phytoplankton size class, Remote Sensing of Environment, 168, 437–450,
         https://doi.org/10.1016/j.rse.2015.07.004, 2015.

Buitenhuis, E. T., Hashioka, T., and Quéré, C. L.: Combined constraints on global ocean primary production using observations and models,
         Global Biogeochemical Cycles, 27, 847–858, https://doi.org/10.1002/gbc.20074, 2013a.

480 Buitenhuis, E. T., Vogt, M., Moriarty, R., Bednaršek, N., Doney, S. C., Leblanc, K., Le Quéré, C., Luo, Y.-W., O'Brien, C., O'Brien, T., Peloquin, J., Schiebel, R., and Swan, C.: MAREDAT: towards a world atlas of MARine Ecosystem DATa, Earth System Science Data, 5, 227–239, https://doi.org/10.5194/essd-5-227-2013, 2013b.

Deppeler, S. L. and Davidson, A. T.: Southern Ocean Phytoplankton in a Changing Climate, Frontiers in Marine Science, 4, 40, https://doi.org/10.3389/fmars.2017.00040, 2017.

485 Dutkiewicz, S., Hickman, A. E., Jahn, O., Gregg, W. W., Mouw, C. B., and Follows, M. J.: Capturing optically important constituents and properties in a marine biogeochemical and ecosystem model, Biogeosciences, 12, 4447–4481, https://doi.org/10.5194/bg-12-4447-2015, 2015.

Dutkiewicz, S., Hickman, A. E., and Jahn, O.: Modelling ocean-colour-derived chlorophyll a, Biogeosciences, 15, 613–630, https://doi.org/10.5194/bg-15-613-2018, 2018.

490 Follows, M. J., Dutkiewicz, S., Grant, S., and Chisholm, S. W.: Emergent Biogeography of Microbial Communities in a Model Ocean, Science, 315, 1843–1846, https://doi.org/10.1126/science.1138544, 2007.

Garcia, H. E., Locarnini, R. A., Boyer, T. P., Antonov, J. I., Baranova, O., Zweng, M., Reagan, J., and Johnson, D.: Dissolved Inorganic Nutrients (phosphate, nitrate, silicate), in: World Ocean Atlas 2013 Volume 4, edited by Levitus, S. and Mishonov, A., p. 25 pp, NOAA Atlas NESDIS 76, 2014.

495 Geider, R. J., Maclntyre, H. L., and Kana, T. M.: A dynamic regulatory model of phytoplanktonic acclimation to light, nutrients, and temperature, Limnology and Oceanography, 43, 679–694, https://doi.org/10.4319/lo.1998.43.4.0679, 1998.

Gregg, W. W. and Casey, N. W.: Modeling coccolithophores in the global oceans, Deep Sea Research Part II: Topical Studies in Oceanography, 54, 447–477, https://doi.org/10.1016/j.dsr2.2006.12.007, the Role of Marine Organic Carbon and Calcite Fluxes in Driving Global Climate Change, Past and Future, 2007.

500 Gregg, W. W. and Rousseaux, C. S.: Directional and Spectral Irradiance in Ocean Models: Effects on Simulated Global Phytoplankton, Nutrients, and Primary Production, Frontiers in Marine Science, 3, 240, https://doi.org/10.3389/fmars.2016.00240, 2016.

Group, M.: MITgcm Manual, 2012.

Hashioka, T., Vogt, M., Yamanaka, Y., Le Quéré, C., Buitenhuis, E. T., Aita, M. N., Alvain, S., Bopp, L., Hirata, T., Lima, I., Sailley, S., and Doney, S. C.: Phytoplankton competition during the spring bloom in four plankton functional type models, Biogeosciences, 10,
505 6833–6850, https://doi.org/10.5194/bg-10-6833-2013, 2013.

Hauck, J., Arrigo, K. R., Hoppema, M., van Dijken, G. L., Völker, C., and Wolf-Gladrow, D. A.: Insignificant buffering capacity of Antarctic shelf carbonates, Global Biogeochemical Cycles, 27, 11–20, https://doi.org/10.1029/2011GB004211, 2013.

Hickman, A. E., Dutkiewicz, S., Williams, R. G., and Follows, M. J.: Modelling the effects of chromatic adaptation on phytoplankton community structure in the oligotrophic ocean, Marine Ecology Progress Series, 406, 1 – 17, https://doi.org/10.3354/meps08588, 2010.

510 Hirata, T., Hardman-Mountford, N. J., Brewin, R. J. W., Aiken, J., Barlow, R., Suzuki, K., Isada, T., Howell, E., Hashioka, T., Noguchi-Aita, M., and Yamanaka, Y.: Synoptic relationships between surface Chlorophyll-a and diagnostic pigments specific to phytoplankton functional types, Biogeosciences, 8, 311–327, https://doi.org/10.5194/bg-8-311-2011, 2011.

Hiscock, M. R., Lance, V. P., Apprill, A. M., Bidigare, R. R., Johnson, Z. I., Mitchell, B. G., Smith, W. O., and Barber, R. T.: Photosynthetic maximum quantum yield increases are an essential component of the Southern Ocean phytoplankton response to iron, Proceedings of the
515 National Academy of Sciences, 105, 4775–4780, https://doi.org/10.1073/pnas.0705006105, 2008.

Huskin, I., Anadon, R., /'Anadon-Marqu/'es, F., and Harris, R.: Ingestion, faecal pellet and egg production rates of Calanus helgolandicus feeding coccoliphophorid versus non-coccolithophorid diets, J. Exp. Mar. Biol. Ecol., pp. 239–254, 2000.

Iglesias-Rodríguez, M. D., Brown, C. W., Doney, S. C., Kleypas, J., Kolber, D., Kolber, Z., Hayes, P. K., and Falkowski, P. G.: Representing key phytoplankton functional groups in ocean carbon cycle models: Coccolithophorids, Global Biogeochemical Cycles, 16, 47–1–47–20,

520   https://doi.org/10.1029/2001GB001454, 2002.

Janjić, T., Bormann, N., Bocquet, M., Carton, J. A., Cohn, S. E., Dance, S. L., Losa, S. N., Nichols, N. K., Potthast, R., Waller, J. A., and Weston, P.: On the representation error in data assimilation, Quarterly Journal of the Royal Meteorological Society, 144, 1257–1278, https://doi.org/10.1002/qj.3130, 2018.

Kaufman, D. E., Friedrichs, M. A. M., Smith Jr., W. O., Hofmann, E. E., Dinniman, M. S., and Hemmings, J. C. P.: Climate change impacts

525   on southern Ross Sea phytoplankton composition, productivity, and export, Journal of Geophysical Research: Oceans, 122, 2339–2359, https://doi.org/10.1002/2016JC012514, 2017.

Kobayashi, S., Ota, Y., Harada, Y., Ebita, A., Moriya, M., Onoda, H., Onogi, K., Kamahori, H., Kobayashi, C., Endo, H., Miyaoka, K., and Takahashi, K.: The JRA-55 Reanalysis: General Specifications and Basic Characteristics, Journal of the Meteorological Society of Japan. Ser. II, 93, 5–48, https://doi.org/10.2151/jmsj.2015-001, 2015.

530 Laufkötter, C., Vogt, M., Gruber, N., Aita-Noguchi, M., Aumont, O., Bopp, L., Buitenhuis, E., Doney, S. C., Dunne, J., Hashioka, T., Hauck, J., Hirata, T., John, J., Le Quéré, C., Lima, I. D., Nakano, H., Seferian, R., Totterdell, I., Vichi, M., and Völker, C.: Drivers and uncertainties of future global marine primary production in marine ecosystem models, Biogeosciences, 12, 6955–6984, https://doi.org/10.5194/bg-12-6955-2015, 2015.

Le Quéré, C., Harrison, S. P., Colin Prentice, I., Buitenhuis, E. T., Aumont, O., Bopp, L., Claustre, H., Cotrim Da Cunha, L., Geider, R.,

535   Giraud, X., Klaas, C., Kohfeld, K. E., Legendre, L., Manizza, M., Platt, T., Rivkin, R. B., Sathyendranath, S., Uitz, J., Watson, A. J., and Wolf-Gladrow, D.: Ecosystem dynamics based on plankton functional types for global ocean biogeochemistry models, Global Change Biology, 11, 2016–2040, https://doi.org/10.1111/j.1365-2486.2005.1004.x, 2005.

Leblanc, K., Arístegui, J., Armand, L., Assmy, P., Beker, B., Bode, A., Breton, E., Cornet, V., Gibson, J., Gosselin, M.-P., Kopczynska, E., Marshall, H., Peloquin, J., Piontkovski, S., Poulton, A. J., Quéguiner, B., Schiebel, R., Shipe, R., Stefels, J., van Leeuwe, M. A., Varela,

540   M., Widdicombe, C., and Yallop, M.: A global diatom database – abundance, biovolume and biomass in the world ocean, Earth System Science Data, 4, 149–165, https://doi.org/10.5194/essd-4-149-2012, 2012.

Longhurst, A.: Ecological Geography of the Sea, Academic press, 1998.

Losa, S., Soppa, M. A., Dinter, T., Wolanin, A., Brewin, R. J. W., Bricaud, A., Oelker, J., Peeken, I., Gentili, B., Rozanov, V. V., and Bracher, A.: Global data sets of Chlorophyll a concentration for diatoms, coccolithophores (haptophytes) and cyanobacteria obtained

545   from in situ observations and satellite retrievals, https://doi.org/10.1594/PANGAEA.873210, https://doi.org/10.1594/PANGAEA.873210, supplement to: Losa, S et al. (2017): Synergistic Exploitation of Hyper- and Multi-Spectral Precursor Sentinel Measurements to Determine Phytoplankton Functional Types (SynSenPFT). Frontiers in Marine Science, 4(203), 22 pp, https://doi.org/10.3389/fmars.2017.00203, 2017.

Losa, S. N., Vézina, A., Wright, D., Lu, Y., Thompson, K., and Dowd, M.: 3D ecosystem modelling in the North Atlantic: Relative impacts

550   of physical and biological parameterizations, Journal of Marine Systems, 61, 230–245, https://doi.org/10.1016/j.jmarsys.2005.09.011, workshop on Future Directions in Modelling Physical-Biological Interactions (WKFDPBI), 2006.

Losa, S. N., Soppa, M. A., Dinter, T., Wolanin, A., Brewin, R. J. W., Bricaud, A., Oelker, J., Peeken, I., Gentili, B., Rozanov, V., and Bracher, A.: Synergistic Exploitation of Hyper- and Multi-Spectral Precursor Sentinel Measurements to Determine Phytoplankton Functional Types (SynSenPFT), Frontiers in Marine Science, 4, 203, https://doi.org/10.3389/fmars.2017.00203, 2017.

555 Losa, S. N., Oelker, J., Soppa, M. A., Losch, M., Dutkiewicz, S., Dinter, T., Richter, A., Rozanov, V. V., Burrows, J. P., and Bracher,
     A.: Investigating the phytoplankton diversity in the Great Calcite Belt: perspective from modelling and satellite retrievals, in: Extended
     Abstract, Ocean Optics Conference XXIV, Dubrovnik (Croatia), 7 October 2018 - 12 October 2018, https://oceanopticsconference.org/
     extended/Losa_Svetlana.pdf, 2018.

Menemenlis, D., Campin, J.-M., Heimbach, P., Hill, C., Lee, T., Nguyen, A., Schodlock, M., and Zhang, H.: High resolution global ocean
560   and sea ice data synthesis, Mercator Ocean Quartely Newsletter, 31, 13–21, 2008.

Milliman, J. D.: Production and accumulation of calcium carbonate in the ocean: Budget of a nonsteady state, Global Biogeochemical Cycles,
     7, 927–957, https://doi.org/10.1029/93GB02524, 1993.

Moisan, T. A. and Mitchell, B. G.: Modeling Net Growth of Phaeocystis antarctica Based on Physiological and Optical Responses to Light
     and Temperature Co-limitation, Frontiers in Marine Science, 4, 437, https://doi.org/10.3389/fmars.2017.00437, 2018.

565 Morán, X. A. G., Fernández, E., and Pérez, V.: Size-fractionated primary production, bacterial production and net community pro-
     duction in subtropical and tropical domains of the oligotrophic ne atlantic in autumn, Marine Ecol. Progr. Ser., 274, 17–29,
     https://doi.org/10.3354/meps274017, 2004.

Mouw, C. B., Hardman-Mountford, N. J., Alvain, S., Bracher, A., Brewin, R. J. W., Bricaud, A., Ciotti, A. M., Devred, E., Fujiwara,
     A., Hirata, T., Hirawake, T., Kostadinov, T. S., Roy, S., and Uitz, J.: A Consumer's Guide to Satellite Remote Sensing of Multiple
570   Phytoplankton Groups in the Global Ocean, Frontiers in Marine Science, 4, 41, https://doi.org/10.3389/fmars.2017.00041, 2017.

Nejstgaard, J. C., Gismervik, I., and T., S. P.: Feeding and reproduction by Calanus finmarchicus, and microzooplankton grazing
     during mesocosm blooms of diatoms and the coccolithophore Emiliania huxleyi, Marine Ecology Progress Series, 147, 197–217,
     https://doi.org/10.3354/meps147197, 1997.

Nissen, C., Vogt, M., Münnich, M., Gruber, N., and Haumann, F. A.: Factors controlling coccolithophore biogeography in the Southern
575   Ocean, Biogeosciences, 15, 6997–7024, https://doi.org/10.5194/bg-15-6997-2018, https://www.biogeosciences.net/15/6997/2018/, 2018.

O'Brien, C. J., Peloquin, J. A., Vogt, M., Heinle, M., Gruber, N., Ajani, P., Andruleit, H., Arístegui, J., Beaufort, L., Estrada, M., Karentz, D.,
     Kopczyńska, E., Lee, R., Poulton, A. J., Pritchard, T., and Widdicombe, C.: Global marine plankton functional type biomass distributions:
     coccolithophores, Earth System Science Data, 5, 259–276, https://doi.org/10.5194/essd-5-259-2013, 2013.

Orsi, A. H. and Harris, U.: Locations of the various fronts in the Southern Ocean Australian Antarctic Data Centre – CAASM Metadata,
580   https://data.aad.gov.au/metadata/records/southern_ocean_fronts, updated 2015, 2001.

Orsi, A. H., Whitworth, T., and Nowlin, W. D.: On the meridional extent and fronts of the Antarctic Circumpolar Current, Deep Sea Research
     Part I: Oceanographic Research Papers, 42, 641 – 673, https://doi.org/10.1016/0967-0637(95)00021-W, 1995.

Paasche, E.: A review of the coccolithophorid Emiliania huxleyi (Prymnesiophyceae), with particular reference to growth, coccolith forma-
     tion, and calcification-photosynthesis interactions, Phycologia, 40, 503–529, https://doi.org/10.2216/i0031-8884-40-6-503.1, 2001.

585 Peloquin, J., Swan, C., Gruber, N., Vogt, M., Claustre, H., Ras, J., Uitz, J., Barlow, R., Behrenfeld, M., Bidigare, R., Dierssen, H., Ditullio,
     G., Fernandez, E., Gallienne, C., Gibb, S., Goericke, R., Harding, L., Head, E., Holligan, P., Hooker, S., Karl, D., Landry, M., Letelier, R.,
     Llewellyn, C. A., Lomas, M., Lucas, M., Mannino, A., Marty, J.-C., Mitchell, B. G., Muller-Karger, F., Nelson, N., O'Brien, C., Prezelin,
     B., Repeta, D., Jr. Smith, W. O., Smythe-Wright, D., Stumpf, R., Subramaniam, A., Suzuki, K., Trees, C., Vernet, M., Wasmund, N., and
     Wright, S.: The MAREDAT global database of high performance liquid chromatography marine pigment measurements, Earth System
590   Science Data, 5, 109–123, https://doi.org/10.5194/essd-5-109-2013, 2013.

Platt, T., Gallegos, C. L., and Harrison, W. G.: Photoinhibi- tion of photosynthesis in natural assemblages of marine phytoplankton, J. mar
     Res., pp. 687–701, 1980.

Popova, E., Fasham, M., Osipov, A., and Ryabchenko, V.: Chaotic behaviour of an ocean ecosystem model under seasonal external forcing, Journal of Plankton Research, 19, 1495–1515, https://doi.org/10.1093/plankt/19.10.1495, 1997.

595 Popova, E., Pollard, R., Lucas, M., Venables, H., and Anderson, T.: Real-time forecasting of ecosystem dynamics during the CROZEX experiment and the roles of light, iron, silicate, and circulation, Deep Sea Research Part II: Topical Studies in Oceanography, 54, 1966 – 1988, https://doi.org/10.1016/j.dsr2.2007.06.018, the Crozet Natural Iron Bloom and Export Experiment, 2007.

Queguiner, B.: Iron fertilization and the structure of planktonic communities in high nutrient regions of the Southern Ocean, Deep Sea Research Part II: Topical Studies in Oceanography, 90, 43–54, https://doi.org/10.1016/j.dsr2.2012.07.024, https://hal.archives-ouvertes.

600 fr/hal-02086574, 2013.

Rost, B. and Riebesell, U.: Coccolithophores and the biological pump: responses to environmental changes, in: Coccolithophores: from molecular processes to global impact, edited by Thiestern, H. R. and Young, J. R., pp. 99–125, Springer, Berlin, 2004.

Sadeghi, A., Dinter, T., Vountas, M., Taylor, B. B., Altenburg-Soppa, M., Peeken, I., and Bracher, A.: Improvement to the PhytoDOAS method for identification of coccolithophores using hyper-spectral satellite data, Ocean Science, 8, 1055–1070, https://doi.org/10.5194/os-8-1055-

605 2012, 2012.

Sathyendranath, S.: Phytoplankton functional types from Space, in: Reports of the International Ocean-Colour Coordinating Group (IOCCG), vol. 15, pp. 1–156, International Ocean-Colour Coordinating Group, 2014.

Schartau, M., Engel, A., Schröter, J., Thoms, S., Völker, C., and Wolf-Gladrow, D.: Modelling carbon overconsumption and the formation of extracellular particulate organic carbon, Biogeosciences, 4, 433–454, https://doi.org/10.5194/bg-4-433-2007, 2007.

610 Schourup-Kristensen, V., Sidorenko, D., Wolf-Gladrow, D. A., and Völker, C.: A skill assessment of the biogeochemical model REcoM2 coupled to the Finite Element Sea Ice–Ocean Model (FESOM 1.3), Geoscientific Model Development, 7, 2769–2802, https://doi.org/10.5194/gmd-7-2769-2014, 2014.

Shang, S., Wu, J., Huang, B., Lin, G., Lee, Z., Liu, J., and Shang, S.: A new approach to discriminate dinoflagellate from diatom blooms from space in the East China Sea, Journal of Geophysical Research: Oceans, 119, 4653–4668, https://doi.org/10.1002/2014JC009876, 2014.

615 Signorini, S. R., Garcia, V. M. T., Piola, A. R., Garcia, C. A. E., Mata, M. M., and McClain, C. R.: Seasonal and interannual variability of calcite in the vicinity of the Patagonian shelf break (38°S–52°S), Geophysical Research Letters, 33, https://doi.org/10.1029/2006GL026592, 2006.

Smith, H. E. K., Poulton, A. J., Garley, R., Hopkins, J., Lubelczyk, L. C., Drapeau, D. T., Rauschenberg, S., Twining, B. S., Bates, N. R., and Balch, W. M.: The influence of environmental variability on the biogeography of coccolithophores and diatoms in the Great Calcite Belt,

620 Biogeosciences, 14, 4905–4925, https://doi.org/10.5194/bg-14-4905-2017, 2017.

Soppa, M., Losa, S., Brewin, R., Bricaud, A., and Bracher, A.: SynSenPFT Product Validation report (PVR):Version 3.3, https://www.awi.de/fileadmin/user_upload/AWI/Forschung/Klimawissenschaft/Physikalische_Ozeanographie_der_Polarmeere/ SEOM-SynSenPFT-PVR-D2.4_v3.3.pdf, 2016a.

Soppa, M. A., Hirata, T., Silva, B., Dinter, T., Peeken, I., Wiegmann, S., and Bracher, A.: Global Retrieval of Diatom Abundance Based on

625 Phytoplankton Pigments and Satellite Data, Remote Sensing, 6, 10089–10106, https://doi.org/10.3390/rs61010089, 2014.

Soppa, M. A., Völker, C., and Bracher, A.: Diatom Phenology in the Southern Ocean: Mean Patterns, Trends and the Role of Climate Oscillations, Remote Sensing, 8, https://doi.org/10.3390/rs8050420, 2016b.

Soppa, M. A., Peeken, I., and Bracher, A.: Global chlorophyll a concentrations for diatoms, haptophytes and prokaryotes obtained with the Diagnostic Pigment Analysis of HPLC data compiled from several databases and individual cruises,

630 https://doi.org/10.1594/PANGAEA.875879, https://doi.org/10.1594/PANGAEA.875879, in supplement to: Losa, Svetlana; Soppa, Mari-

ana A; Dinter, Tilman; Wolanin, Aleksandra; Brewin, Robert J W; Bricaud, Annick; Oelker, Julia; Peeken, Ilka; Gentili, Bernard; Rozanov, Vladimir V; Bracher, Astrid (2017): Synergistic Exploitation of Hyper- and Multi-Spectral Precursor Sentinel Measurements to Determine Phytoplankton Functional Types (SynSenPFT). Frontiers in Marine Science, 4(203), 22 pp, https://doi.org/10.3389/fmars.2017.00203, 2017.

635   Taylor, M. H., Losch, M., and Bracher, A.: On the drivers of phytoplankton blooms in the Antarctic marginal ice zone: A modeling approach, Journal of Geophysical Research: Oceans, 118, 63–75, https://doi.org/10.1029/2012JC008418, 2013.

Trimborn, S., Hoppe, C. J., Taylor, B. B., Bracher, A., and Hassler, C.: Physiological characteristics of open ocean and coastal phytoplankton communities of Western Antarctic Peninsula and Drake Passage waters, Deep Sea Research Part I: Oceanographic Research Papers, 98, 115 – 124, https://doi.org/10.1016/j.dsr.2014.12.010, 2015.

640   Tréguer, P., Bowler, C., Moriceau, B., Dutkiewicz, S., Gehlen, M., Aumont, O., Bittner, L., Dugdale, R., Finkel, Z., Iudicone, D., Jahn, O., Guidi, L., Lasbleiz, M., Leblanc, K., Levy, M., and Pondaven, P.: Influence of diatom diversity on the ocean biological carbon pump, Nature Geoscience, 11, 27 – 37, https://doi.org/10.1038/s41561-017-0028-x, 2018.

Uitz, J., Claustre, H., Morel, A., and Hooker, S. B.: Vertical distribution of phytoplankton communities in open ocean: An assessment based on surface chlorophyll, Journal of Geophysical Research: Oceans, 111, https://doi.org/10.1029/2005JC003207, 2006.

645   Vidussi, F., Claustre, H., Manca, B. B., Luchetta, A., and Marty, J.-C.: Phytoplankton pigment distribution in relation to upper thermocline circulation in the eastern Mediterranean Sea during winter, Journal of Geophysical Research: Oceans, 106, 19 939–19 956, https://doi.org/10.1029/1999JC000308, 2001.

Vogt, M., O'Brien, C., Peloquin, J., Schoemann, V., Breton, E., Estrada, M., Gibson, J., Karentz, D., Van Leeuwe, M. A., Stefels, J., Widdicombe, C., and Peperzak, L.: Global marine plankton functional type biomass distributions: Phaeocystis spp., Earth System Science Data, 650   4, 107–120, https://doi.org/10.5194/essd-4-107-2012, 2012.

Vogt, M., Hashioka, T., Payne, M. R., Buitenhuis, E. T., Quéré, C. L., Alvain, S., Aita, M. N., Bopp, L., Doney, S. C., Hirata, T., Lima, I., Sailley, S., and Yamanaka, Y.: The distribution, dominance patterns and ecological niches of plankton functional types in Dynamic Green Ocean Models and satellite estimates, Biogeosciences Discussions, 10, 17 193–17 247, https://doi.org/10.5194/bgd-10-17193-2013, https://www.biogeosciences-discuss.net/10/17193/2013/, 2013.

655   Ward, B. A., Dutkiewicz, S., Jahn, O., and Follows, M. J.: A size-structured food-web model for the global ocean, Limnology and Oceanography, 57, 1877–1891, https://doi.org/10.4319/lo.2012.57.6.1877, 2012.

Ward, B. A., Marañón, E., Sauterey, B., Rault, J., and Claessen, D.: The Size Dependence of Phytoplankton Growth Rates: A Trade-Off between Nutrient Uptake and Metabolism, The American Naturalist, 189, 170–177, https://doi.org/10.1086/689992, pMID: 28107051, 2017.

660   Waterbury, J. B., Watson, S. W., Valois, F. W., and Franks, D. G.: Biological and ecological characterization of the marine unicellular cyanobacterium synechococcus, Can. Bull. Fish Aquat. Sci., 214, 120, 1986.

Xi, H., Losa, S. N., Mangin, A., Soppa, M. A., Garnesson, P., Demaria, J., d'Andon, O. H. F., and Bracher, A.: Global Retrieval Algorithms for Phytoplankton Functional Types (PFTs): toward the Applications to OLCI and GlobColour Merged Products, in: Extended Abstract, Ocean Optics Conference XXIV, Dubrovnik (Croatia), 7 October 2018 - 12 October 2018, https://oceanopticsconference.org/extended/ 665   Xi_Hongyan.pdf, 2018.

Table 1. Biogeochemical model internal parameters/traits settings with *Phaeo* for *Phaeocystis*, *Prochlor* for *Prochlorococcus*, Nfixer for nitrogen fixing PFT and coccolith for coccolithophores

Param\PFTs	Large diatom	*Phaeo*	small diatoms	*Prochlor*	Nfixer	coccolith
P^C_{max}	1.79	1.59	2.16	1.09	0.31	1.23
β				1.25		
k_{sat_N}	0.451	0.106	0.053	0.007	0.0	0.086
k_{sat_P}	0.028	0.007	0.003	0.0004	0.004	0.0054
$k_{sat_{Fe}}$, $*10^{-3}$	0.028	0.007	0.0033	0.0005	0.0124	0.0054
$r_{j,k=1}$	0.8	0.78	0.2	0.2	0.6	0.58
$r_{j,k=2}$	0.16	0.156	1.0	1.0	0.12	0.12
w_{sink}	0.77	0.23	0.10	0.03	0	0.23
$mfunc$	silicified		silicified			calcifier

Table 2. Table of specification of the key phytoplankton groups (PG) given their biomineralizing function (BF) and size class as referred in the observations (PSC) and model (SCM).

PG	PSC in situ	SCM	BF
Diatoms	micro/nano	"large"/"small"	silicified
large cells	micro	"large"	strong silicified
smal cells	nano	"small euk"	weak silicified
Haptophytes	nano/pico	"other large"	
Phaeocystis	nano/pico	"other large"	
coccolithophores	nano	"large"	calcifier
Prokaryotes	pico		
N-fixer	pico	small	
Prochlorococcus	pico	"other small"	

pico < 2 μm; 2μm < nano < 20 μm; micro > 20 μm

Table 3. Diatoms: model *vs. in situ* statistics at Longhurst's provinces

criteria\bioms	APLR	ANTA	SANT	SSTC	CHIL	FKLD	EAFR	AUSW	AUSE
MAE ($mgChla\ m^{-3}$)	1.00	0.75	0.27	0.08	0.27	0.15	0.21	0.01	0.03
RMSE ($mgChla\ m^{-3}$)	1.90	1.44	0.41	0.13	0.42	0.21	0.42	0.02	0.05
RMSE unbiased	1.88	1.34	0.39	0.13	0.35	0.18	0.40	0.02	0.05
bias ($mgChla\ m^{-3}$)	-0.29	0.52	-0.12	0	-0.22	-0.11	-0.13	0	0
N	1287	235	402	102	24	12	6	7	19

MAE – mean absolute error ($mgChla\ m^{-3}$); RMSE — root mean squared error ($mgChla\ m^{-3}$); bioms are the Longhurst's biogeochemical provinces (Longhurst, 1998): Austral Polar Province (APLR), Antarctic Province (ANTA), Subantarctic Water Ring Province (SANT), South Subtropical Convergence Province (SSTC), Humbold Current Coastal Province (CHIL), Southwest Atlantic Shelves Province (FKLD), Eastern Africa Coastal Province (EAFR), Australia-Indonesia Coastal Province (AUSW), East Australian Coastal Province (AUSE).

Table 4. Haptophytes: model *vs. in situ* statistics at Longhurst's provinces

criteria\bioms	APLR	ANTA	SANT	SSTC	CHIL	FKLD	EAFR	AUSW	AUSE
MAE ($mgChla\ m^{-3}$)	0.24	0.22	0.16	0.14	0.19	0.13	0.57	0.10	0.48
RMSE ($mgChla\ m^{-3}$)	0.45	0.27	0.21	0.25	0.24	0.18	0.85	0.15	0.53
RMSE unbiased	0.44	0.26	0.21	0.26	0.22	0.17	0.62	0.12	0.22
bias ($mgChla\ m^{-3}$)	0.01	0.01	-0.10	-0.03	-0.08	-0.07	0.57	0.09	0.48
N	1264	229	437	154	26	12	12	23	39

Same as in Table 3

Table 5. Prokaryotes model *vs. in situ* statistics at Longhurst's provinces

criteria \bioms	APLR	ANTA	SANT	SSTC	CHIL	FKLD	EAFR	AUSW	AUSE
MAE ($mgChla\ m^{-3}$)	0.28	0.11	0.06	0.14	0.08	0.06	0.05	0.07	0.05
RMSE($mgChla\ m^{-3}$)	0.64	0.19	0.13	0.22	0.13	0.08	0.05	0.08	0.05
RMSE unbiased	0.57	0.16	0.12	0.18	0.13	0.06	0.05	0.04	0.05
bias ($mgChla\ m^{-3}$)	-0.23	-0.11	-0.06	-0.13	0	-0.06	-0.02	-0.06	-0.01
N	772	42	201	82	21	7	12	39	27

Same as in Table 3, 4
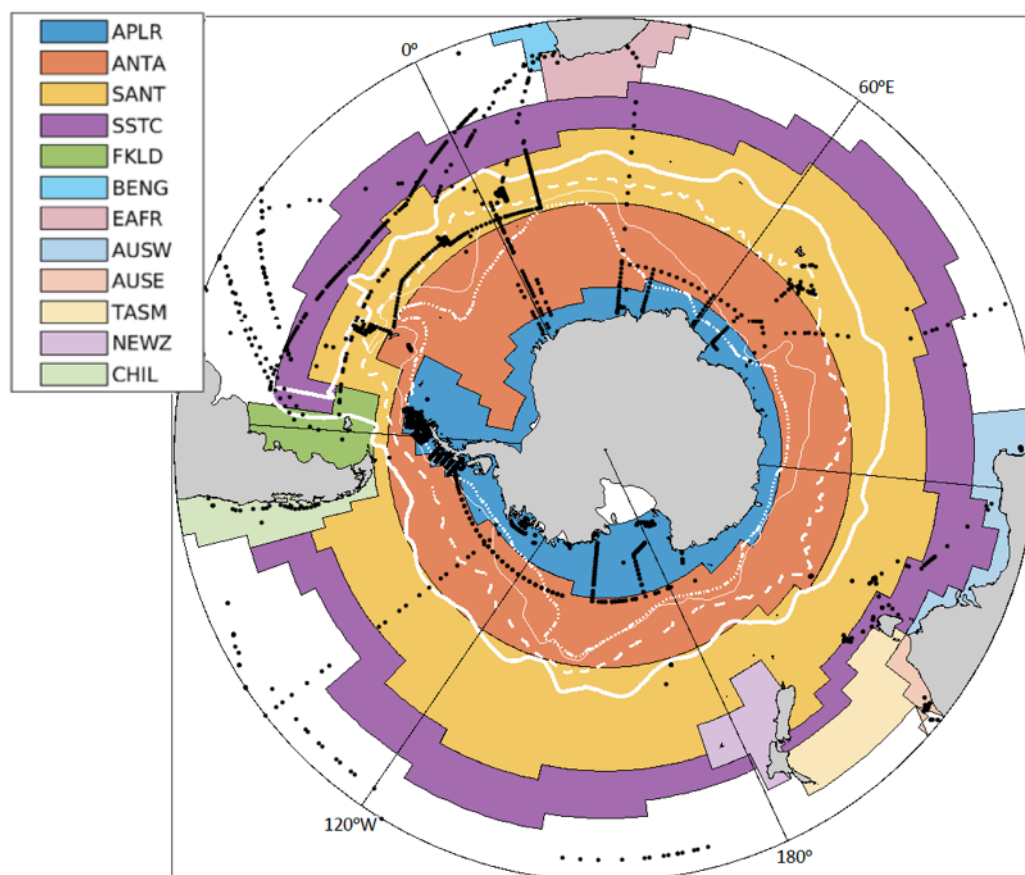
Figure 1. Distribution of *in situ* observations (black dots) over the Longhurst's biogeochemical provinces (coloured domains): Austral Polar Province (APLR), Antarctic Province (ANTA), Subantarctic Water Ring Province (SANT), South Subtropical Convergence Province (SSTC), Humbold Current Coastal Province (CHIL), Southwest Atlantic Shelves Province (FKLD), Eastern Africa Coastal Province (EAFR), Australia-Indonesia Coastal Province (AUSW), East Australian Coastal Province (AUSE). The white curves denote the Southern Ocean fronts (Orsi et al., 1995; Orsi and Harris, 2001): the Sub-Antarctic Front (SAF, thick curve); the Polar Front (PF, dashed), the Southern Antarctic Circumpolar Current Front (SACCF, thin curve) and the Southern Boundary of ACC (SBDY, dotted).

27
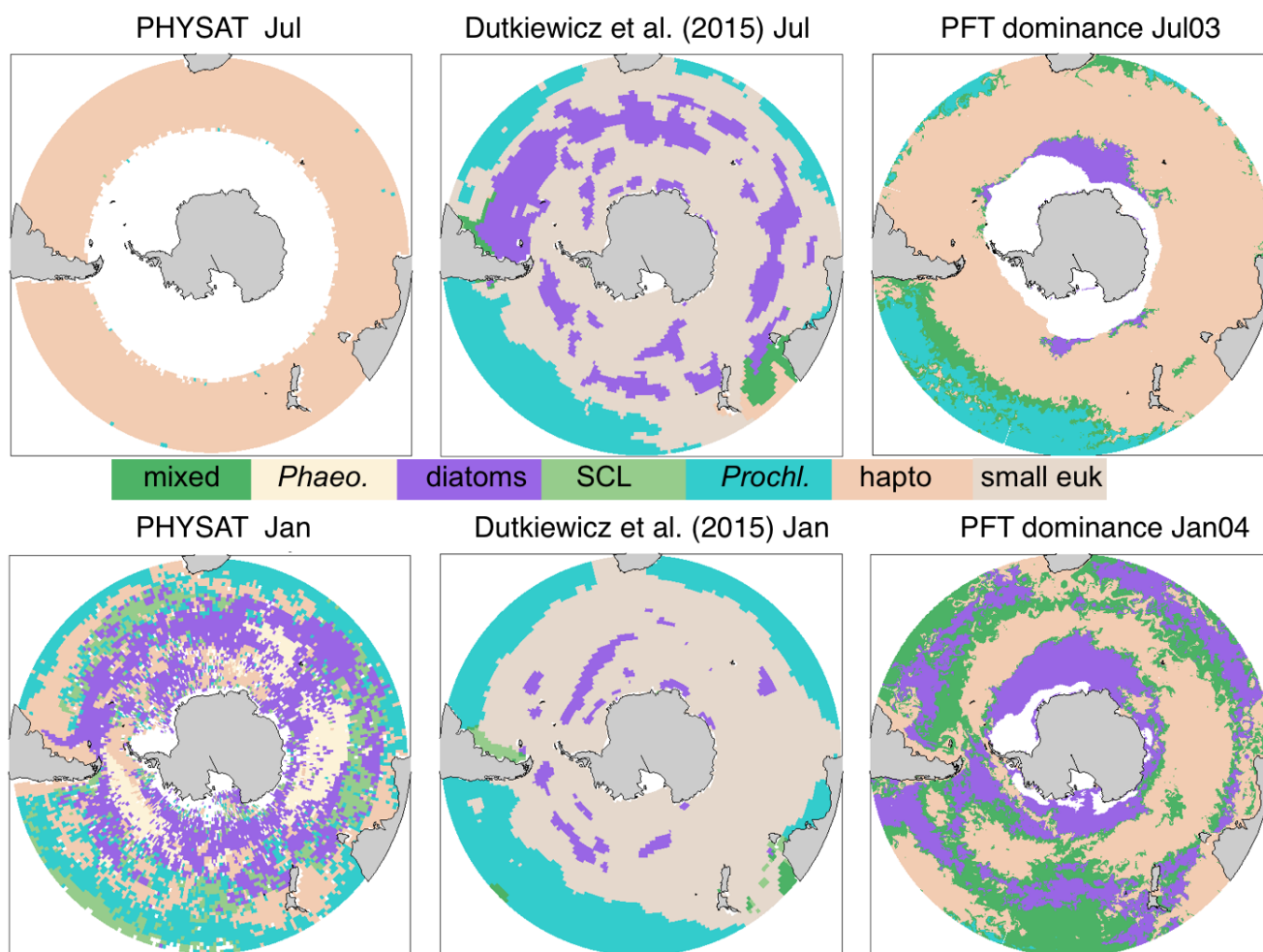
Figure 2. Surface PFT dominance retrieved by PHYSAT algorithm and simulated with the Darwin-MITgcm version of Dutkiewicz et al. (2015) and current model set up for July 2003 and January 2004. "SCL" represents *Synechococcus* like prokaryotic phytoplankton (not considered in current model version). Simulated haptophytes include coccolithophores and *Phaeocystis*. The our model output is masked by the area with sea ice concentration > 75% during respective month. Model PFT is considered dominant if its Chla fraction of total Chla is more than 55%.
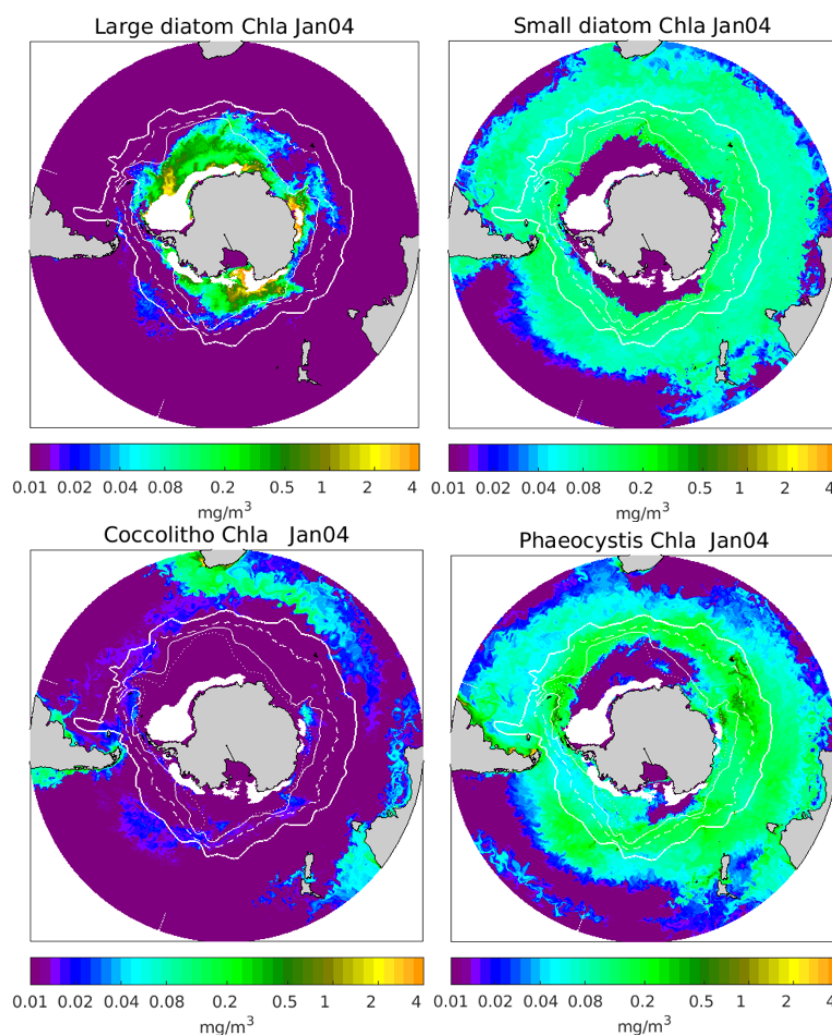
Figure 3. Spatial distribution of the model surface chlorophyll "a" for large and small diatoms, coccolithophores and *Phaeocystis*-analogue ("other large") in the Southern Ocean for January 2004 (experiment REF).
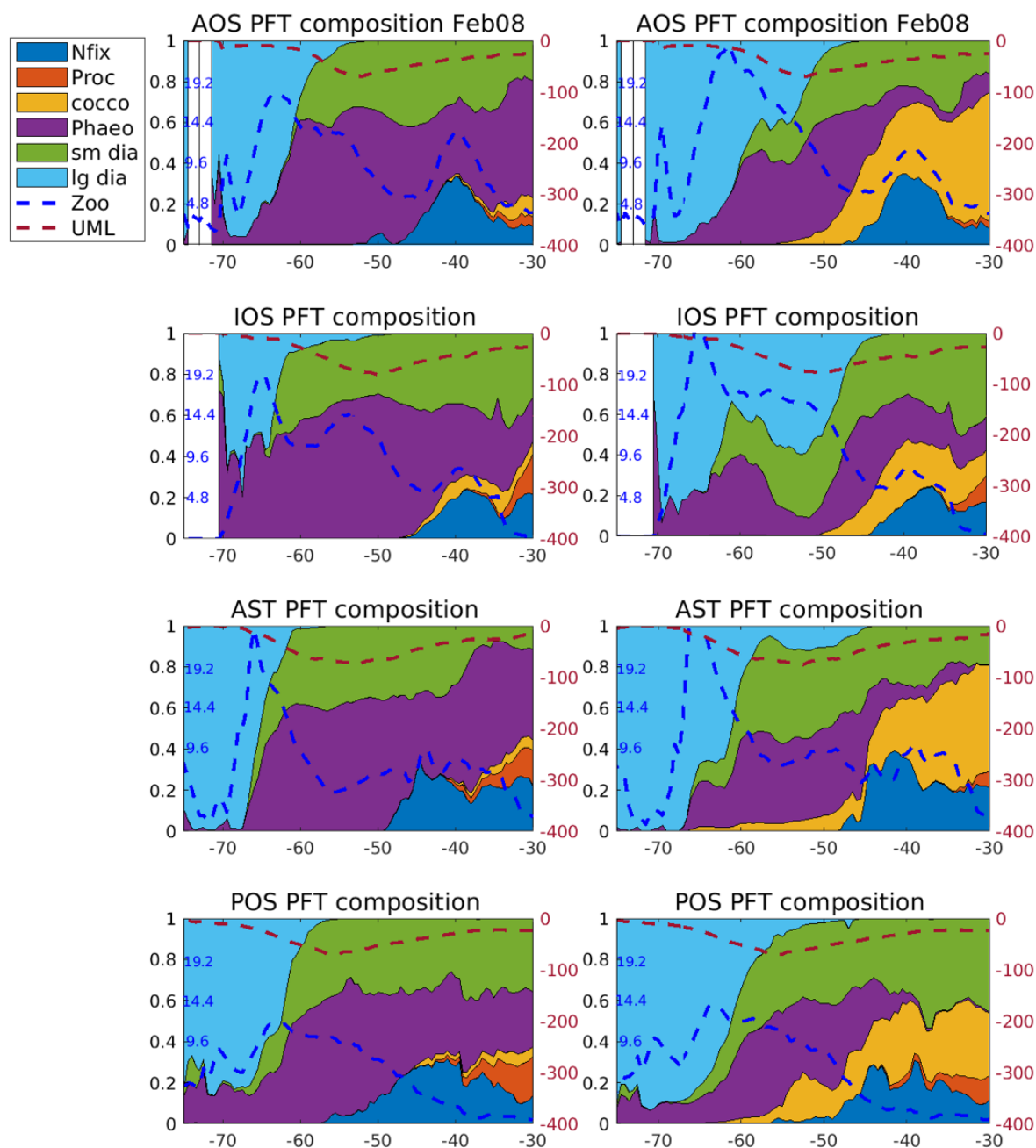
Figure 4. Meridional (from 75°S to 30°S) distribution of zonally averaged phytoplankton composition for the Atlantic Ocean sector (AOS, 60°W – 18°E), the Indian Ocean sector (IOS, 18°E – 120°E), Australian sector (AST, 120°E – 180°E) and the Pacific Ocean sector (POS, 180°E – 60°W) in February 2008. The red dashed curve represents the upper mixed layer depth (zonally averaged, m). The blue curve represents zonally averaged zooplankton concentration (mgC m^{-3}): experiment REF (to the left); experiment PHAEO (to the right). "Cocco" for coccolithophores, "Phaeo" for "other large" (including *Phaeocystis*), "sm dia" for small diatoms and "lg dia" for large diatoms.
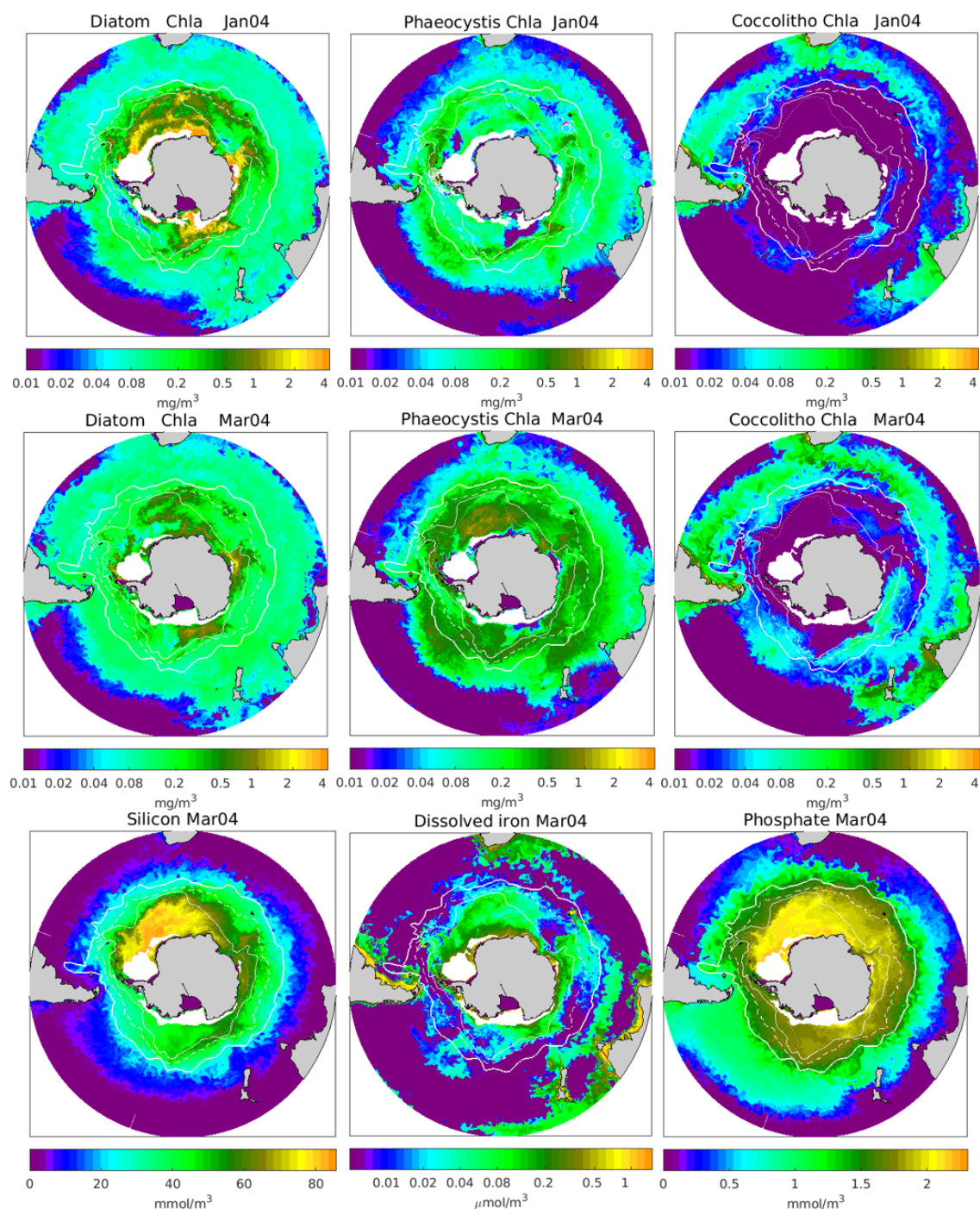
Figure 5. Surface spatial distribution of the model diatoms (small + large), *Phaeocystis* and coccolithophores chlorophyll "a" in the Southern Ocean for January (upper panels) and March 2004 (experiment PHAEO, middle panels). Lower panes: March 2004 spatial distribution of surface silicon, phosphate and dissolved iron for experiment PHAEO.
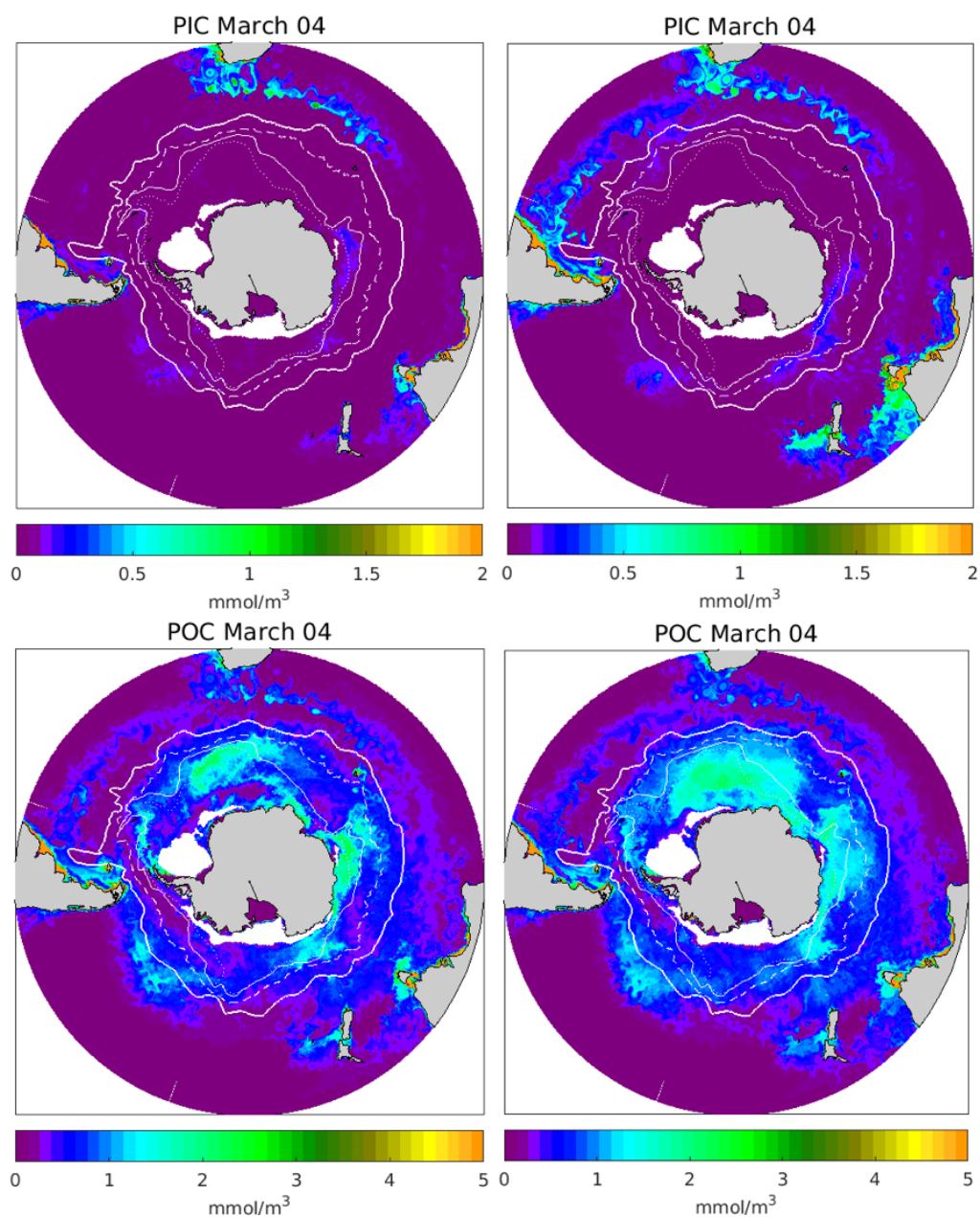
Figure 6. Spatial distribution of the model Surface particulate inorganic carbon (PIC, upper panels) and particulate organic carbon (POC, lower panels) in the Southern Ocean for two experiments in March 2004: experiment REF (to the left); experiment PHAEO (to the right).
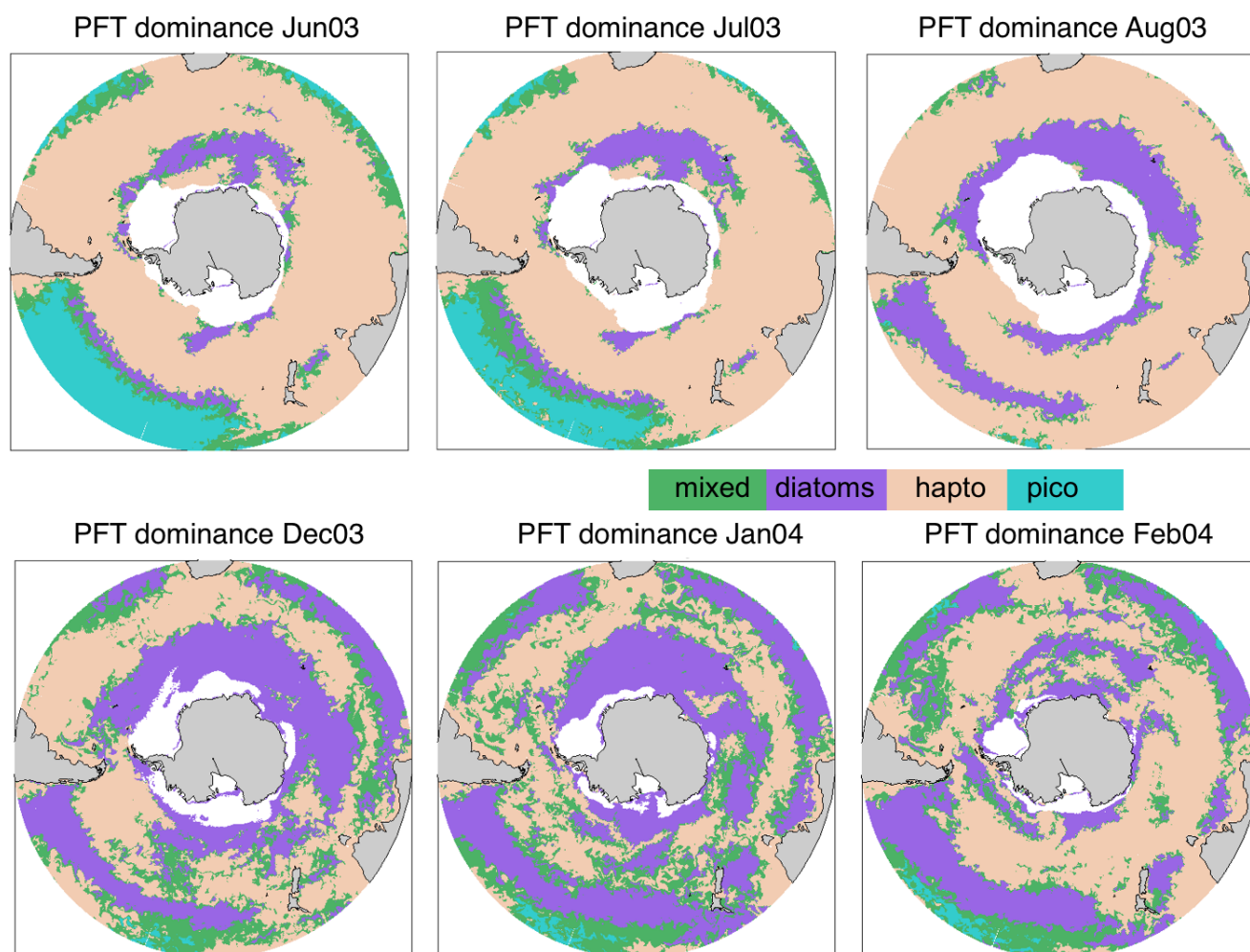
Figure 7. The surface PFT dominance simulated with Darwin-MITgcm for 2003/2004 for experiment PHAEO. Pico represents prokaryotes. The our model output is masked by the area with sea ice concentration > 75% during respective month. Model PFT is considered dominant if its Chla fraction of total Chla is more than 55%.
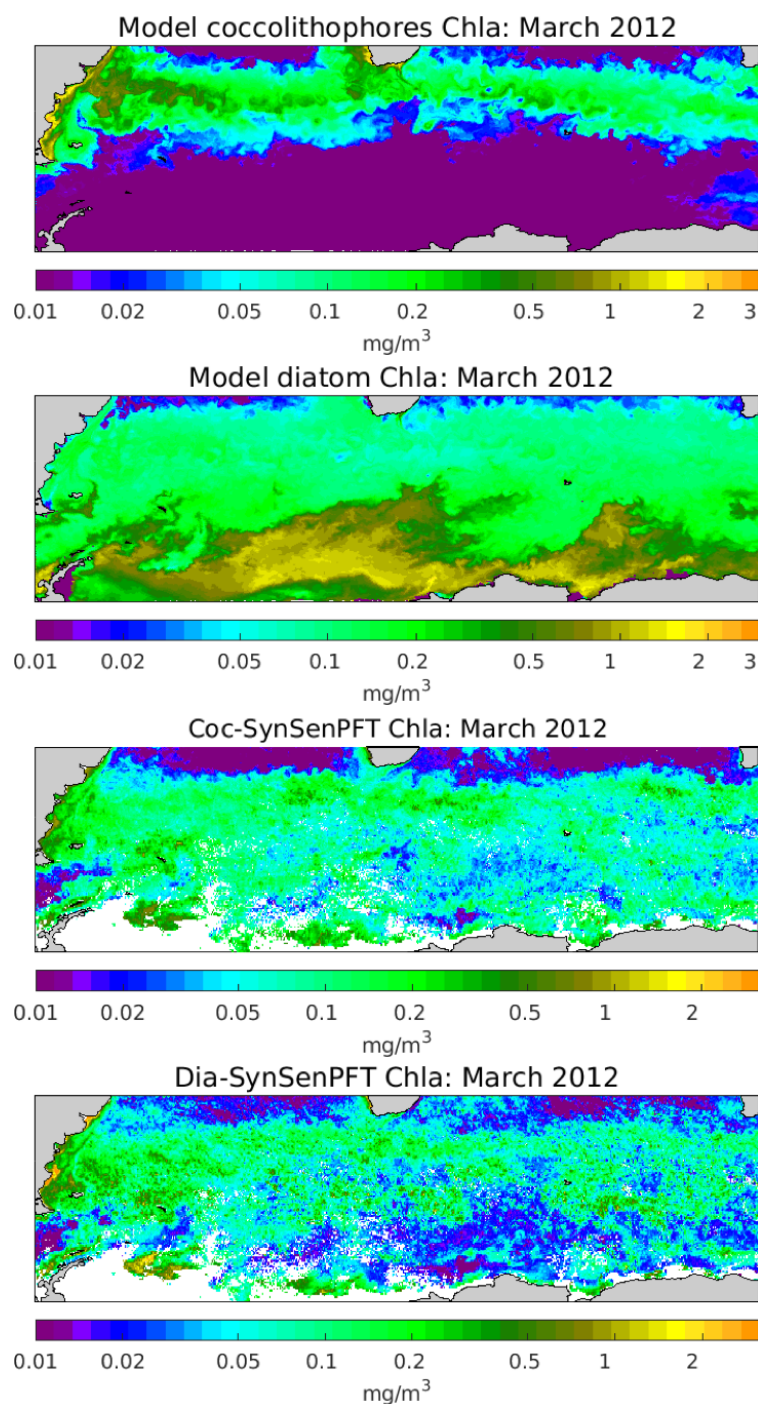
Figure 8. The surface Chla for coccolithophores and diatoms as model simulated (two upper panels) and retrieved with SynSenPFT algorithm (two lower panels) distributed over the domain shown by Smith et al. (2017) for March 2012.
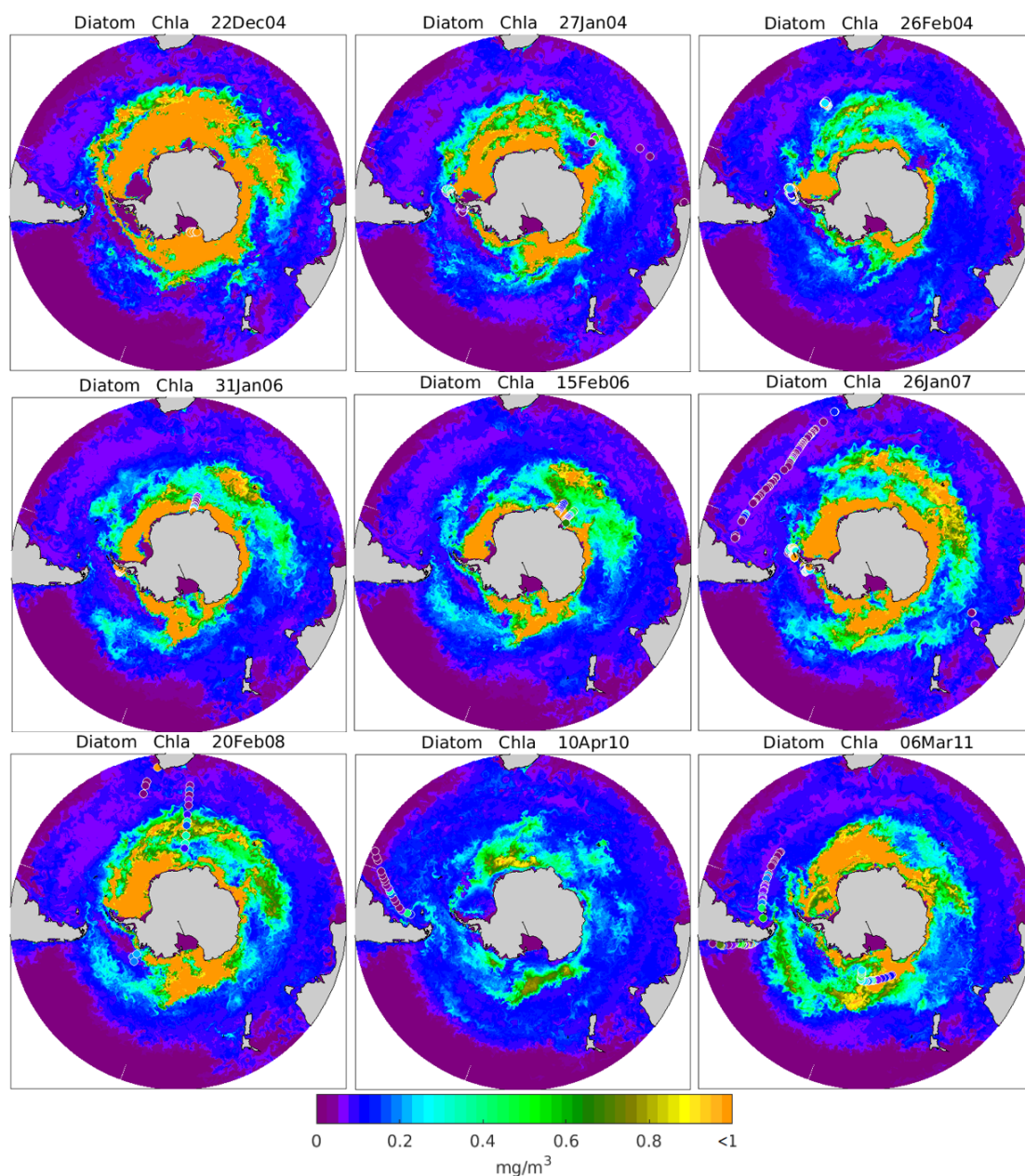
Figure 9. Simulated surface diatoms Chla shown for several model snapshots and compared against *in situ* observations (circles).
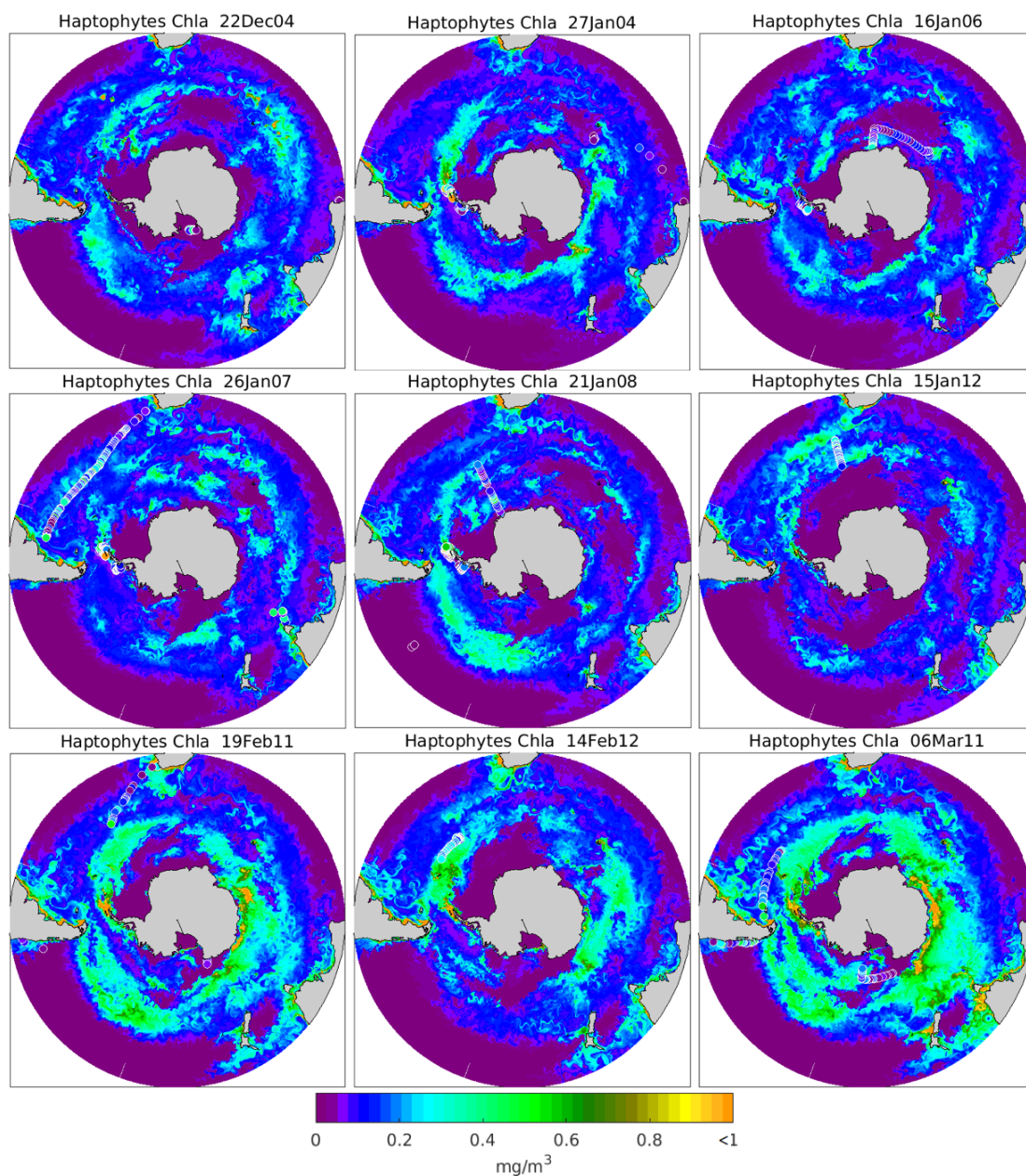
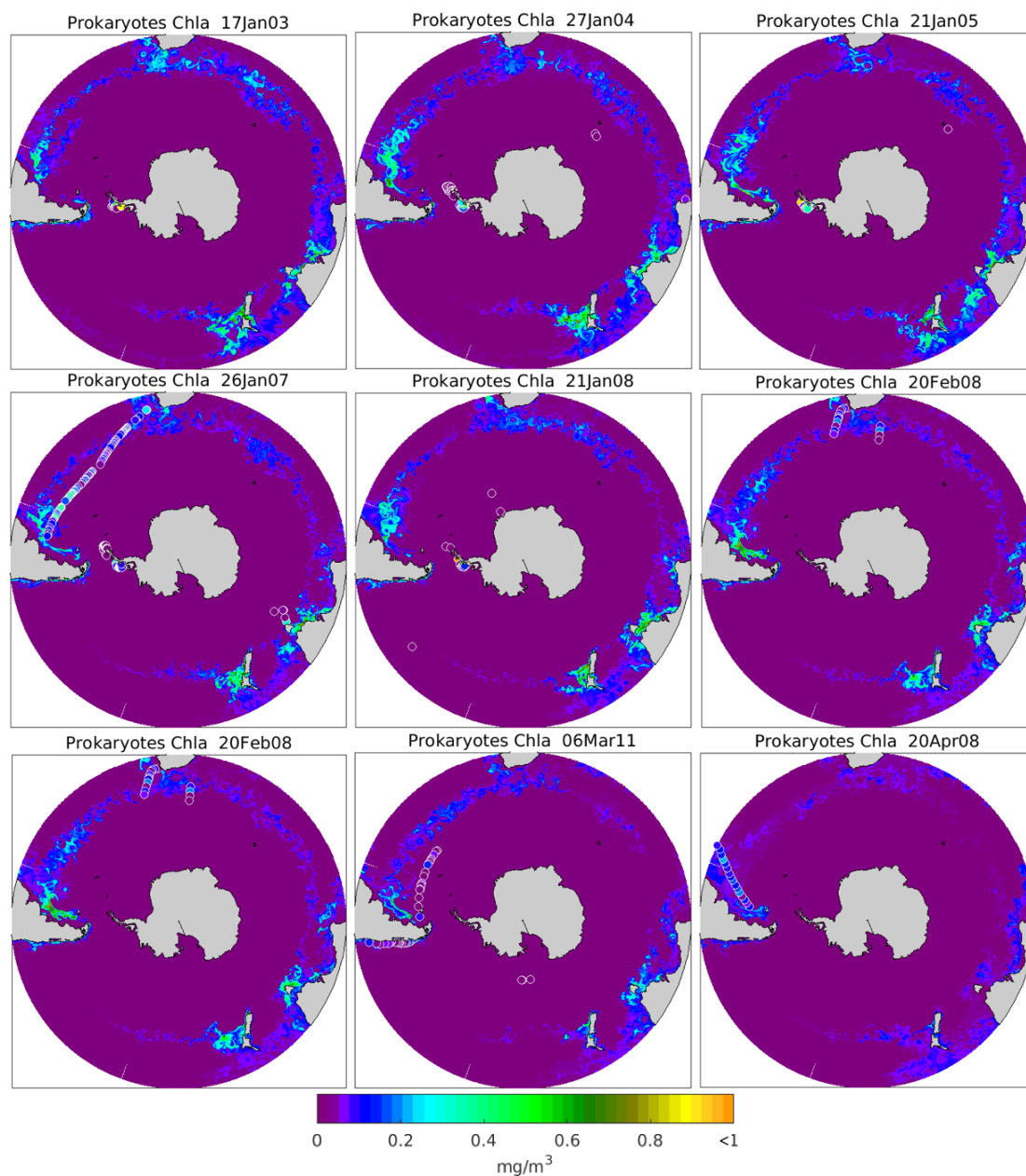**Figure 10.** Same as Figure 9 but for haptophytes.

Figure 11. Same as Figures 9 and 10 but for prokaryotes.